SUPPLEMENTAL DATA

ASCE *Journal of Geotechnical and Geoenvironmental Engineering*

Forensic Geotechnical Analyses on the 2009 Building-Overturning Accident in Shanghai, China: Beyond Common Recognitions

Yong Tan, Wei-Zhen Jiang, Hai-Sheng Rui, Ye Lu, and Da-Long Wang

DOI: 10.1061/(ASCE)GT.1943-5606.0002264

www.ascelibrary.org

Fig. S1. Three-dimensional (3D) view of the site investigated.

Theoretical Calculation of Stockpiling Effect on Adjacent Building 7

Theoretical calculations were carried out to evaluate adverse effect of the soil stockpiles on the piles underneath building 7. Under the additional vertical earth pressures, $\Delta\sigma_v$, generated by the stockpile (surcharge), the subgrade below building 7 would have undergone compression and the settlement of the subsoil relative to the piles would have produced downdrag force, Q_n, on the piles. In the analyses, the trapezoidal cross-section of the 10-m high stockpile behind building 7 was simplified as an equivalent uniformly distributed strip load, q, (5.75-m high rectangular stockpile). The soil stockpiles had a unit weight about 16.5 $\mathrm{kN/m^3}$ and thus $q = 16.5\ \mathrm{kN/m^3} \times 5.75\ \mathrm{m} = 94.88\ \mathrm{kP}$.

Then, $\Delta\sigma_v$, due to the stockpile was estimated by Boussinesq solution (Terzaghi 1943), refer to Fig. S2, i.e.,

$$\Delta\sigma_v = \frac{q}{\pi}\left[\beta_1 + \frac{1}{2}\sin 2\beta_1 - \beta_2 - \frac{1}{2}\sin 2\beta_2\right] \quad \text{(S1)}$$

The estimated $\Delta\sigma_v$ along depth at the locations of piles closest to the stockpile, pile (north), and furthest from the stockpile, pile (south), were summarized in Tables S1 and S2.

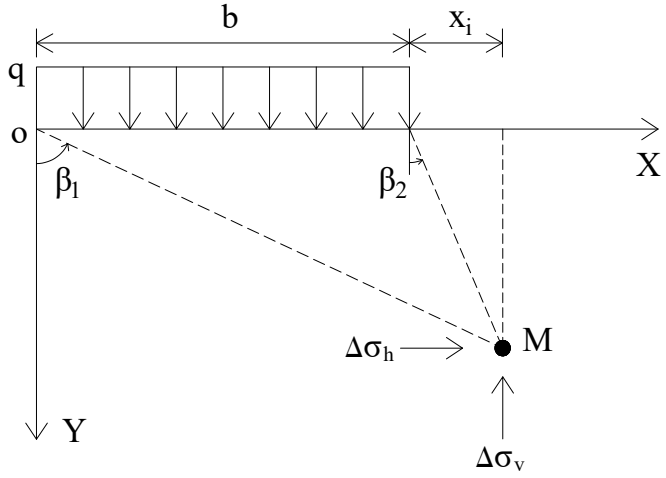

Fig. S2. Schematic illustration of Boussinesq solution.

Table S1. Summary of the estimated $\Delta\sigma_v$ along depth at pile (north).

Y (m)	x_i (m)	b + x_i	q (kPa)	β_1	β_2	$\Delta\sigma_v$ (kPa)
0	2	42	94.9	/	/	0.00
1	2	42	94.9	1.54	1.11	1.92
1.3	2	42	94.9	1.53	0.99	3.61
2	2	42	94.9	1.51	0.79	8.62
3.5	2	42	94.9	1.46	0.52	18.74
7.5	2	42	94.9	1.34	0.26	31.94
13.5	2	42	94.9	1.18	0.15	38.03
19.2	2	42	94.9	1.04	0.10	39.66
22.1	2	42	94.9	0.97	0.09	39.82
22.5	2	42	94.9	0.97	0.09	39.82
28	2	42	94.9	0.86	0.07	39.32
29.7	2	42	94.9	0.83	0.07	39.03
32.8	2	42	94.9	0.78	0.06	38.39
35	2	42	94.9	0.75	0.06	37.87
40	2	42	94.9	0.68	0.05	36.52
45	2	42	94.9	0.63	0.04	35.06

Table S2. Summary of the estimated $\Delta\sigma_v$ along depth at pile (south).

Y (m)	x_i (m)	b + x_i	q (kPa)	β_1	β_2	$\Delta\sigma_v$ (kPa)
0	13.6	53.6	94.9	/	/	0.00
1	13.6	53.6	94.9	1.55	1.50	0.01
1.3	13.6	53.6	94.9	1.54	1.48	0.02
2	13.6	53.6	94.9	1.53	1.42	0.06
3.5	13.6	53.6	94.9	1.49	1.32	0.31
7.5	13.6	53.6	94.9	1.40	1.07	2.40
13.5	13.6	53.6	94.9	1.27	0.79	8.21
19.2	13.6	53.6	94.9	1.16	0.62	13.78
22.1	13.6	53.6	94.9	1.11	0.55	16.13
22.5	13.6	53.6	94.9	1.10	0.54	16.43
28	13.6	53.6	94.9	1.01	0.45	19.77
29.7	13.6	53.6	94.9	0.98	0.43	20.56
32.8	13.6	53.6	94.9	0.93	0.39	21.74
35	13.6	53.6	94.9	0.90	0.37	22.41
40	13.6	53.6	94.9	0.84	0.33	23.45
45	13.6	53.6	94.9	0.78	0.29	23.99

Then, the elastic compression of each soil layer, s_i, caused by $\Delta\sigma_v$ was estimated by:

$$s_i = \frac{\Delta\sigma_v}{E_s} H_i \quad \text{(S2)}$$

where, E_s, constrained modulus measured by odometer test (Table 1 of the article); H_i, thickness of each soil layer. The calculated magnitudes of s_i at pile (north) and pile (south) are summarized in Tables S3 and S4.

Then, both pile settlement and downdrag forces on pile due to the ground subsidence can be roughly estimated by determining the location of the neutral plane of a pile where the pile and ground settled equally. The neutral plane was determined at the depth where shaft resistance along a pile changed over from negative skin friction into positive skin friction (Fellenius 1984; 1998). Fig. 8(c) of the article presents the development of downdrag force along depth and the settlement development of the piles and the soils along depth. In the left graph of Fig.8(c), the red line represents the forcing load curve (the dead load $\mathrm{Q_d}$ + the downdrag force $\mathrm{Q_n}$) and the blue line represents the resistance curve (the toe resistance $\mathrm{R_t}$ + positive shaft resistance $\mathrm{R_s}$). The sum of $\mathrm{Q_d}$ and $\mathrm{Q_n}$ was equal to the sum of $\mathrm{R_t}$ and $\mathrm{R_s}$. In this case, the designed load, $\mathrm{Q_d}$, for each pile was 714 kN. Detailed information regarding pile shaft resistance, $\mathrm{R_s}$, and toe resistance, $\mathrm{R_t}$, can refer to the section entitled "*Comprehensive Evaluations on Pile Capacities*" of this supplementary data. In the right graph of Fig.8(c), the red and the blue lines were the elastic compression of pile (north) and pile (south) caused by ($\mathrm{Q_d}$ + $\mathrm{Q_n}$); the red and the blue dash lines were the calculated soil settlements at pile (north) and pile (south) summarized in Tables S3 and S4.

Table S3. The calculated s_i along depth of pile (north).

Y (m)	H_i (m)	$\Delta\sigma_v$ (kPa)	$\Delta\sigma_v^*$ (kPa)	E_s (MPa)	s_i (mm)
0	0.0	0.00	0	0.00	0.00
1.3	1.3	3.61	1.80	4.00	0.59
2	0.7	8.62	6.11	5.61	0.76
3.5	1.5	18.74	13.68	5.61	3.66
7.5	4.0	31.94	25.34	1.30	77.97
13.5	6.0	38.03	34.98	2.20	95.41
19.2	5.7	39.66	38.84	4.40	50.32
22.1	2.9	39.82	39.74	7.25	15.90
22.5	0.4	39.82	39.82	7.25	2.20
28	5.5	39.32	39.57	6.83	31.86
29.7	1.7	39.03	39.18	9.16	7.27
32.8	3.1	38.39	38.71	9.83	12.21
35	2.2	37.87	38.13	9.86	8.51
40	5.0	36.52	37.20	9.86	18.86
45	5.0	35.06	35.79	16.08	11.13
Total	$\sum s_i$ = 337 mm				

Note：$\Delta\sigma_v^*$, the averaged $\Delta\sigma_v$ of each soil layer.

Table S4. The calculated s_i along depth of pile (south).

Y (m)	H_i (m)	$\Delta\sigma_v$ (kPa)	$\Delta\sigma_v^*$ (kPa)	E_s (MPa)	s_i (mm)
0	0.0	0.00	0.00	0.00	0.00
1.3	1.3	0.02	0.01	4.00	0.00
2	0.7	0.06	0.04	5.61	0.00
3.5	1.5	0.31	0.19	5.61	0.05
7.5	4.0	2.40	1.35	1.30	4.17
13.5	6.0	8.21	5.30	2.20	14.46
19.2	5.7	13.78	11.00	4.40	14.24
22.1	2.9	16.13	14.96	7.25	5.98
22.5	0.4	16.43	16.28	7.25	0.90
28	5.5	19.77	18.10	6.80	14.64
29.7	1.7	20.56	20.17	9.16	3.74
32.8	3.1	21.74	21.15	9.83	6.67
35	2.2	22.41	22.08	9.86	4.93
40	5.0	23.45	22.93	9.86	11.63
45	5.0	23.99	23.72	16.08	7.38
Total	$\sum s_i$ = 89 mm				

Note：$\Delta\sigma_v^*$, the averaged $\Delta\sigma_v$ of each soil layer.

As plotted in Fig. 8(c) of the article, the neutral plane was estimated at a depth of 22.1 m with an estimated downdrag force of 671 kN. The estimated maximum load, sum of (Q_d + Q_n) at the neutral plane, was around 1385 kN, which was below the ultimate pile compression capability $R_p = 1783.74$ kN, refer to the section entitled "*Comprehensive Evaluations on Pile Capacities*" of this supplementary data. The settlement at the pile head, Δ_p, was the estimated soil settlement, s_{np}, at the neutral plane plus the elastic compression (Δ_e) of the piles ($\Delta_p = s_{np} + \Delta_e$), which were around 119 mm at pile (north) and 63 mm at pile (south). Δ_e was calculated by equation (S3) as below:

$$\Delta_e = \frac{(Q_d + Q_n)L}{AE} \tag{S3}$$

where, A, area of pile cross section, equal to 0.0804 m^2; E, elastic modulus of pile, equal to 3.8×10^7 kPa; L, pile length, equal to 33 m.

The theoretical calculation results above indicated that: (1) under the compression of the subgrade by stockpile No. 1, the adjacent building would tilt northwards to the stockpile rather than southwards to the excavation; (2) the piles underneath building 7 would be in a safe state under the adjacent 10-m high stockpile and would not experience compression failure.

Calculation of Factor of Safety against Bearing Capacity Failure for both Floodwalls and Stockpiles

Subgrade below the Strip Footing of Floodwall

The additional vertical earth pressure, $\Delta\sigma_v$, on the footing bases of the floodwalls resulting from the adjacent stockpiles were estimated by Boussinesq solution (Terzaghi 1943), refer to Fig. S3.

$$\Delta\sigma_v = \frac{q}{\pi}\left[\beta_1 + \frac{1}{2}\sin 2\beta_1 - \beta_2 - \frac{1}{2}\sin 2\beta_2\right] \quad \text{(S4)}$$

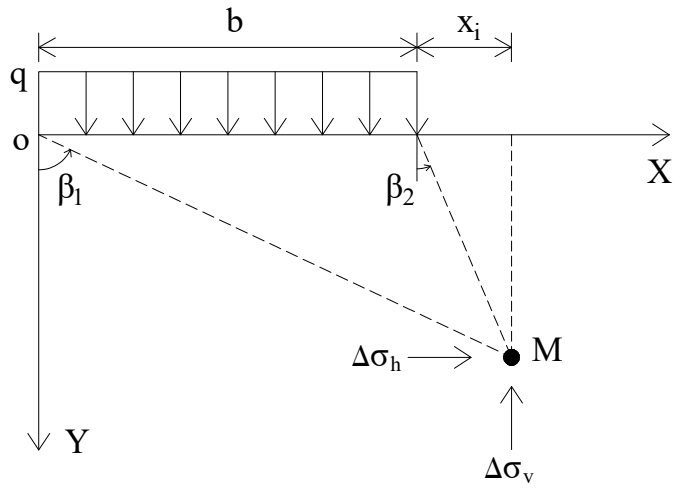

Fig. S3. Schematic illustration of Boussinesq solution.

The calculated maximum $\Delta\sigma_v$ = 4.2 kPa and the minimum $\Delta\sigma_v$ = 2.5 kPa for the floodwall adjacent to stockpile No. 1; the maximum $\Delta\sigma_v$ = 14.4 kPa and the minimum $\Delta\sigma_v$ = 7.9 kPa for the floodwall adjacent to stockpile No. 2. Fig. S4 below plots the distributions of , $\Delta\sigma_v$, at the footing bases of the floodwalls adjacent to stockpiles No. 1 and No. 2.

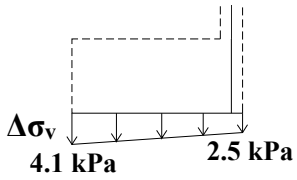

Floodwall footing adjacent to stockpile No. 1 behind building 6

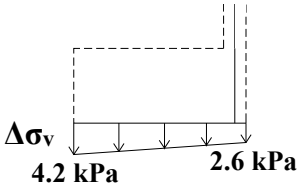

Floodwall footing adjacent to stockpile No. 1 behind building 7

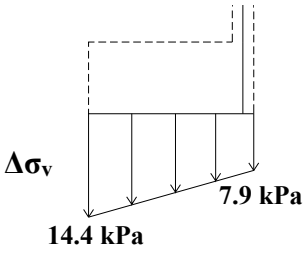

Floodwall footing adjacent to stockpile No. 2

Fig. S4. Distributions of $\Delta\sigma_v$ at the footing bases of the floodwalls adjacent to stockpiles No. 1 and No. 2.

The ultimate bearing capacity, q_{ult}, of the foundation (strip footing) of floodwall was estimated by the general bearing capacity equation proposed by Terzaghi (1943). For an undrained condition, q_{ult}, is equal to:

$$q_{ult} = 5.7S_u + q_s \tag{S5}$$

where, S_u, undrained shear strength of soil; q_s, the weight of soil above the base of the footing. q_s, is calculated by:

$$q_s = \gamma\left(D_f - D\right) + \gamma' D \tag{S6}$$

where, D_f, the depth of the footing below ground level, equal to 7 m; D, the depth of the footing below water level, equal to 4 m; γ, unit weight of soil; γ', effective unit weight of soil. Then, q_s can be calculated by:

$$q_s = 18.5\,kN/m^3 * 1.3\,m + 19.7\,kN/m^3 * 1.7\,m + (19.7 - 10)\,kN/m^3 * 0.5\,m + (15.6 - 10)\,kN/m^3 * 3.5\,m = 82 \text{ kPa} \tag{S7}$$

Then,

$$q_{ult} = 5.7 \times 25\,kPa + 82\,kPa = 224.5\,kPa \tag{S8}$$

If the equation of q_{ult} proposed in Das and Sobhan (2017) for an undrained condition was used, i.e.,

$$q_{ult(net)} = 5.14S_u\left[1 + 0.2\left(\frac{b}{L_f}\right)\right]\left[1 + 0.4\left(\frac{D_f}{b}\right)\right] + q_s \quad \text{(S9)}$$

where, b, width of a strip footing, equal to 2.3 m in this case; L_f, length of strip footing. Because of the large L_f in this case, $\frac{b}{L_f} \approx 0$. Therefore,

$$q_{ult} = 5.14 \times 25\ kPa\left[1 + 0.4\left(\frac{7}{2.3}\right)\right] + 82\ kPa = 367.8\ kPa \quad \text{(S10)}$$

Apparently, the equation of Das and Sobhan (2017) accounting for both shape and depth factors of footing yielded much greater q_{ult} than the equation of Terzaghi (1943). Fig. S4 plots the distribution of additional vertical stresses, $\Delta\sigma_v$, on the footing bases of the floodwalls due to stockpiles No. 1 and No. 2. Therefore, the factor of safety, FS_1, against bearing failure of the floodwall can be estimated by:

$$FS_1 = \frac{q_{ult}}{\Delta\sigma_v + q_s} \quad \text{(S11)}$$

In the case of q_{ult} = 224.5 kPa, the calculated $FS_1 =$ 2.32-2.50 for the floodwall adjacent to stockpile No. 2 and $FS_1 =$ 2.61-2.66 for the floodwall adjacent to stockpile No. 1. If the q_{ult} = 367.8 kPa was used in equation (S11), $FS_1 =$ 3.82-4.09 for the floodwall adjacent to stockpile No. 2 and $FS_1 =$ 4.27-4.35 for the floodwall adjacent to stockpile No. 1.

Subgrade below Stockpiles No. 1 and No. 2

The ultimate bearing capacity, q_{ult}, of the subgrade below the stockpiles at this site was estimated by the method of Liu and Yu (2017), which was developed for surcharge on top thin crust underlain by soft clayey strata like this site. Many failure cases encountered in practice have indicated that for subgrade consisting of top thin crust underlain by soft clayey strata,

punching failure of the top crust followed by general shear failure of the underlying soft strata frequently took place when it was subjected large-scale surcharge (Wei et al. 2012; Liu and Yu 2017). Therefore, a punching failure of the top thin crust followed by a general shear failure of its underlying soft strata was assumed in the method of Liu and Yu (2017). Detailed introduction of this method can refer to Liu and Yu (2017) and will not be repeated herein. The relevant calculation of q_{ult} at this site and evaluation of factor of safety for the subgrade below the stockpiles against bearing capacity failure are briefly introduced in the following sections.

Ultimate bearing capacity of the soft clayey strata underlying the top thin crust

According to Prandtl (1920), the ultimate bearing capacity, q_b, of the soft clayey strata below the top crust can be estimated by:

$$q_b = (\pi + 2)S_u \tag{S12}$$

where, S_u, undrained shear strength. At this site, $S_u = 25$ kPa for the soft clayey strata below the top crust, which was measured by the field vane shear test. It has been widely recognized in literature and practice (Michalowski 1992, 2004; Burd and Frydman 1997; Wei et al. 2012; Liu and Yu 2017) that the existence of top crust would enhance bearing capacity of underlying soft strata to some extent. Hence, q_b of the underlying soft strata can be estimated by equation (S13), in which the top crust outside the loaded area was treated as surcharge on the soft strata.

$$q_b = (\pi + 2)S_u + \gamma H \tag{S13}$$

where, γ, unit weight of top crust; *H*, thickness of top crust.

Load spread angle of top crust

The top crust functioned as a stiff working platform intermediate between the stockpile and the underlying soft strata; thus, the surface load from the stockpile was spread over a wider area (load-spread effect). Consequently, additional pressure resulting from the surcharge onto the underlying soft strata was smaller than that in the absence of the crust. To estimate load-spread angle of the top crust, two soil elements at the boundary of top crust and underlying soft strata (element 1 of the crust and element 2 of the soft strata in Fig. S5) were analyzed in accordance with Mohr-Coulomb theory. When the underlying soft strata reaches the state of limit equilibrium, the principal stress, σ_{ms}, at element 2 is equal to q_b with accounting for the load spread effect, i.e.,

$$\sigma_{ms} = q_b = (\pi + 2)S_u + \gamma H \tag{S14}$$

When the top crust reaches the state of limit equilibrium, the principal stress, σ_{mss}, at element 1 can be assumed that its Mohr-Coulomb stress circle is tangent to the c_{cu}-φ_{cu} envelope of the crust (c_{cu}, cohesion measured by consolidated undrained direct simple-shear test; φ_{cu}, friction angle measured by consolidated undrained direct simple-shear test), see Fig. S6. Thereby, σ_{mss} can be calculated by equation (S15) as below:

$$\sigma_{mss} = (\sigma_{ms} + c_{cu}cos\varphi_{cu}sin\varphi_{cu}) + \sqrt{(c_{cu}cos\varphi_{cu} + \sigma_{ms}sin\varphi_{cu})^2 - (c_{cu}S_u cos\varphi_{cu})^2}/cos^2\varphi_{cu} \tag{S15}$$

Using the graphical method of the state of plane stress, the load spread angle, θ, of the top crust can be obtained as below:

$$\theta = tan^{-1}\left(\frac{\sigma_{mss} - \sigma_{ms} + (\sigma_{mss} + \frac{c_{cu}}{tan\varphi_{cu}})sin^2\varphi_{cu}}{\left(\sigma_{mss} + \frac{c_{cu}}{tan\varphi_{cu}}\right)sin\varphi_{cu}cos\varphi_{cu} + S_u}\right) \tag{S16}$$

Using the soil parameters summarized in Table 1 of the article, the calculated $\theta \approx 45^{\circ}$ at this site.

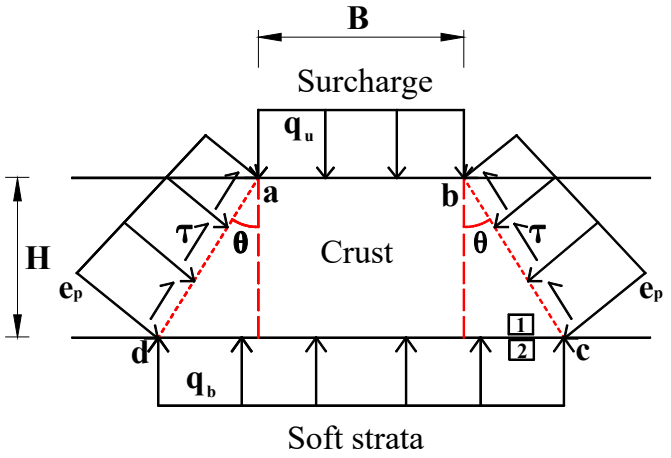

Fig. S5. Conceptual model for calculating load spread angle (redrawn based on Liu and Yu 2017).

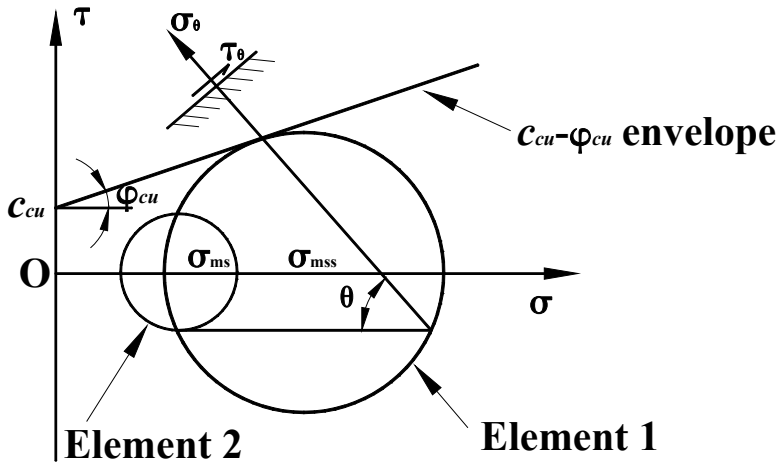

Fig. S6. Mohr-Coulomb stress circles of points 1 and 2 (redrawn based on Liu and Yu 2017).

Ultimate bearing capacity of top crust underlain by soft strata

If the top crust underwent a punching failure under surcharge, the earth pressure, e_p, on its load spread boundaries (i.e., lines ad and bc in Fig. S5) would be in the passive state, which can be calculated by equation (S17) as below:

$$E_p = \int_0^H e_p dz/cos\theta = \int_0^H \frac{(\sigma_z K_p + 2c_{cu}\sqrt{K_p})cos\theta dz}{cos\theta} = \frac{1}{2}\gamma H^2 K_p + 2c_{cu}H\sqrt{K_p} \quad \text{(S17)}$$

where, σ_z, vertical soil stress at depth, z; $K_p = tan^2(45^\circ + \frac{\varphi_{cu}}{2})$. Then, shear force, Q, on

line ab or cd can be calculated by equation (S18):

$$Q = \int_0^H \left(c_{cu} + e_p tan\varphi_{cu}\right) dz/cos\theta = \int_0^H \left[c_{cu} + (\sigma_z K_p + 2c_{cu}\sqrt{K_p})cos\theta\right] tan\varphi_{cu} dz/cos\theta = c_{cu}H/cos\theta + (\frac{1}{2}\gamma H^2 K_p + 2c_{cu}H\sqrt{K_p})tan\varphi_{cu} \quad \text{(S18)}$$

At the state of the static equilibrium, equation (S19) should be satisfied for the punching block abcd, i.e.,

$$q_u B = q_b(B + 2Htan\theta) + 2Qcos\theta - 2E_p sin\theta - \gamma H(B + Htan\theta) \quad \text{(S19)}$$

By inputting equations (S17) and (S18) into equation (S19), ultimate bearing capacity, q_{ult}, of the top crust overlying soft strata can be given by equation (S20):

$$q_{ult} = [(\pi + 2)S_u + \gamma H]\left(1 + 2\frac{H}{B}tan\theta\right) + \frac{H}{B}cos\theta\left(\gamma H K_p + 4c_{cu}\sqrt{K_p}\right) \cdot (tan\varphi_{cu} - tan\theta) + 2c_{cu}\frac{H}{B} - \gamma H(1 + \frac{H}{B}tan\theta) \quad \text{(S20)}$$

in which, *H*, thickness of top crust; *B*, width of surcharge.

Factor of safety against bearing capacity failure

For estimating safety factor, FS_2, of the subgrade below the stockpiles against bearing capacity failure, the trapezoid distributed surface loads of the stockpiles behind buildings 6-7 and 10-11 were simplified as uniformly distributed strip loads for calculation. Figs. S7 to S9 schematically illustrate the equivalent uniform loads, q, of the stockpiles behind these buildings. Then, FS_2 can be calculated by:

$$FS_2 = q_{ult}/q \quad \text{(S21)}$$

The calculated FS_2 magnitudes for the subgrade below the stockpiles behind buildings 6-7 and 10-11 are summarized in Table S5.

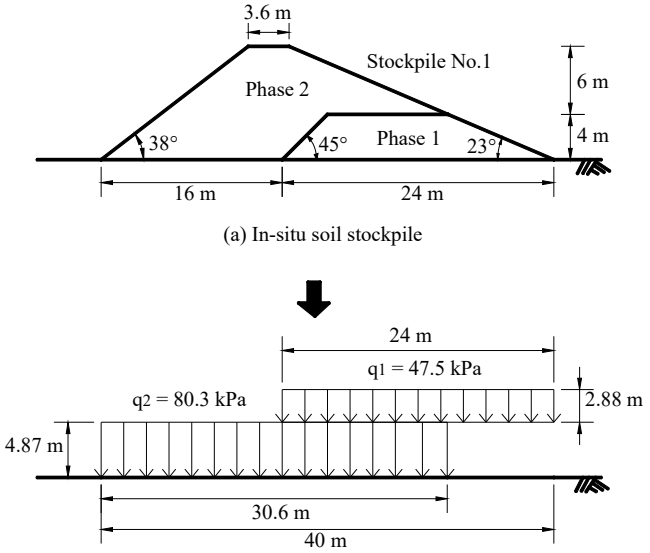

Fig. S7. Simplified models for calculating equivalent load from stockpile No. 1 behind building 6.

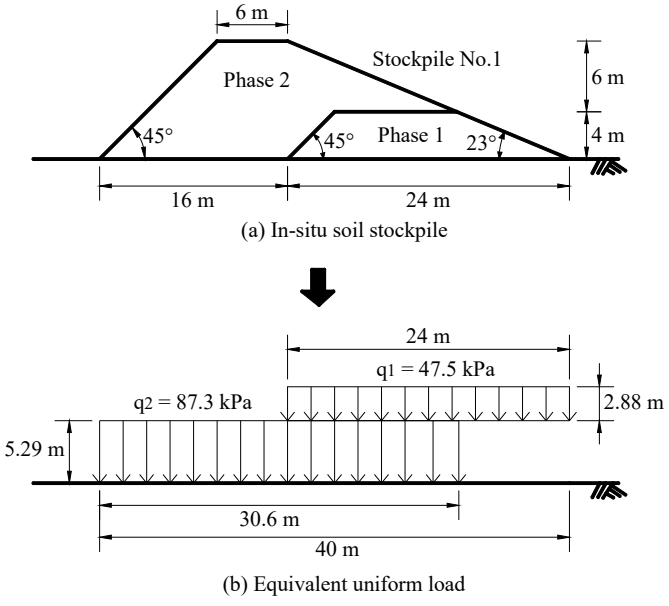

Fig. S8. Simplified models for calculating equivalent load from stockpile No. 1 behind building 7.

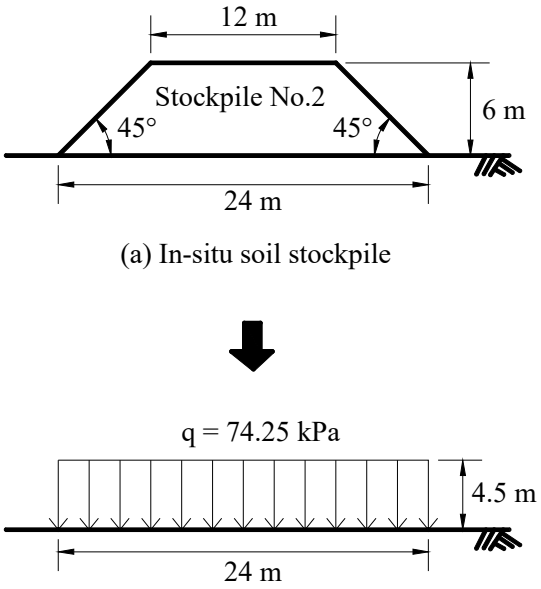

Fig. S9. Simplified models for calculating equivalent load from stockpile No. 2 behind buildings 10-11.

Table S5. Summary of FS_2 for the subgrade below stockpiles No.1 and No.2.

Location	Stockpile	q_{ult} (kPa)	q (kPa)	FS_2
Building 6	Phase 1 of stockpile No.1 (4-m high)	165.3	47.5	3.5
	Phase 2 of stockpile No.1 (10-m high)	150.6	127.8	1.2
Building 7	Phase 1 of stockpile No.1 (4-m high)	165.3	47.5	3.5
	Phase 2 of stockpile No.1 (10-m high)	150.6	134.8	1.1
Buildings 10-11	Stockpile No. 2 (6-m high)	163.1	74.3	2.2

Calculation of Factors of Safety against Sliding and Overturning Failures of Floodwall

Calculation of Lateral Earth Pressures against Floodwall

The floodwall along the Dingpu River consisted of 0.3 m thick and 7.6 m high cantilever concrete wall with a footing of 2.3 m wide and 1 m thick, which had an embedment depth of 2.5 m below the riverbed, see Fig. S10.

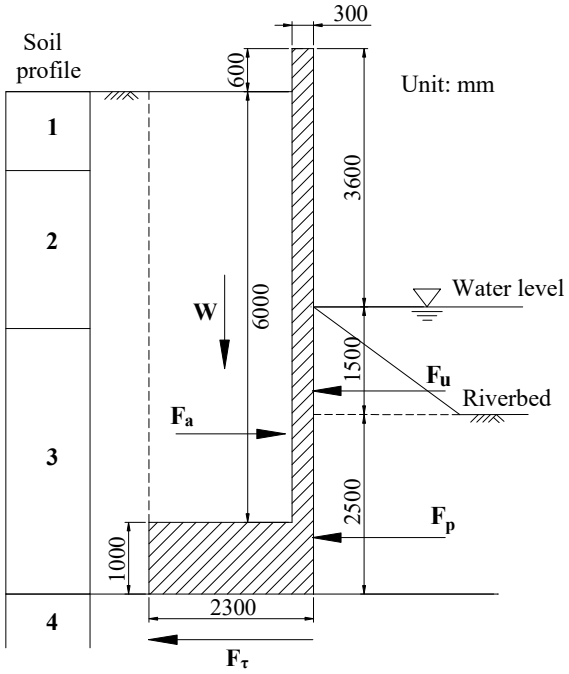

Fig. S10. Simplified calculation model of floodwall.

When the floodwall was approaching sliding or overturning failure, the soil mass behind it was in an active state and the soil mass in front of it was in a passive state. The lateral active earth pressure pushing the floodwall northwards, σ_a, and the lateral passive earth pressure resisting floodwall sliding, σ_p, were calculated according to Rankine earth pressure theory,

i.e.,

$$\sigma_a = \sigma_v \cdot K_a - 2 \cdot c_{cu} \cdot \sqrt{K_a} \quad \text{(S22)}$$

$$\sigma_p = \sigma_v \cdot K_p + 2 \cdot c_{cu} \cdot \sqrt{K_p} \quad \text{(S23)}$$

Where, σ_v, vertical soil stress; $K_a = tan^2(45^\circ - \varphi_{cu}/2)$, lateral active earth pressure coefficient; $K_p = tan^2(45^\circ + \varphi_{cu}/2)$, lateral passive earth pressure coefficient; c_{cu}, soil cohesion measured by consolidated undrained direct simple-shear test (CUDSST); φ_{cu}, soil friction angle measured by CUDSST. The additional lateral and vertical earth pressures, $\Delta\sigma_h$ and $\Delta\sigma_v$, in the subsoils resulting from the stockpiles to the south of floodwall were estimated by Boussinesq solution (Terzaghi 1943), refer to Fig. S11.

$$\Delta\sigma_v = \frac{q}{\pi}\left[\beta_1 + \frac{1}{2}\sin 2\beta_1 - \beta_2 - \frac{1}{2}\sin 2\beta_2\right] \quad \text{(S24)}$$

$$\Delta\sigma_h = \frac{q}{\pi}\left[\beta_1 - \frac{1}{2}\sin 2\beta_1 - \beta_2 + \frac{1}{2}\sin 2\beta_2\right] \quad \text{(S25)}$$

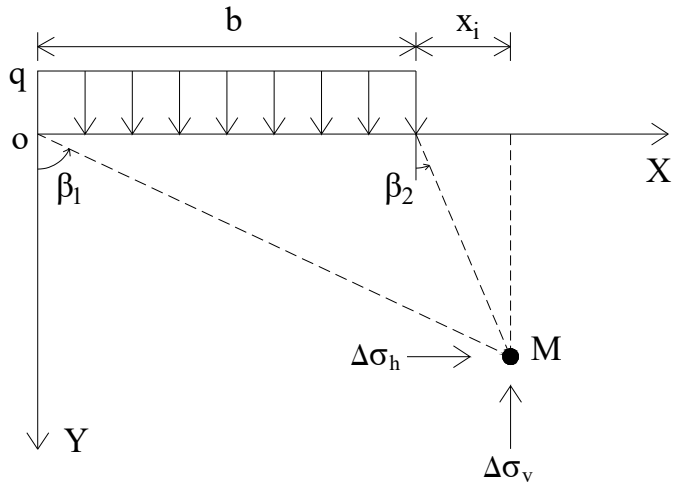

Fig. S11. Schematic illustration of Boussinesq solution.

Estimation on Factors of Safety against Sliding and Overturning Failures of Floodwall

The factor of safety against sliding failure, FS_3, for floodwall can be calculated by equation (S26) as below:

$$FS_3 = \frac{F_\tau + F_u + F_p}{F_a} \quad \text{(S26)}$$

where, F_τ, shear resistance on the bottom of floodwall footing; F_u, thrust of the water pressure above the riverbed against the front side of floodwall; F_p, thrust of lateral Rankine passive earth pressure below the riverbed against the front (north) side of floodwall; F_a, thrust of lateral Rankine active earth pressure and stockpile-induced additional lateral earth pressure against the back (south) side of floodwall. F_τ was estimated by the equation proposed by Chinese Code for Design of Urban Flooding Control Project – GB/T 50805-2012 (2012) as below:

$$F_\tau = \left(c_{cu} + \left(\Delta\sigma_v + \frac{W}{b}\right) \cdot \tan\varphi_{cu}\right) \cdot b \quad \text{(S27)}$$

in which, c_{cu}, soil cohesion measured by CUDSST; φ_{cu}, soil friction angle measured by CUDSST; $\Delta\sigma_v$, additional vertical earth pressure at floodwall footing due to stockpile estimated by equation (S24); W, the weights of floodwall and the soil mass directly above floodwall footing; b, width of floodwall footing.

The factor of safety against overturning failure, FS_4, for floodwall can be calculated by equation (S28) as below:

$$FS_4 = \frac{M_d}{M_r} = \frac{M_W + M_u + M_p}{M_a} \quad \text{(S28)}$$

where, M_d, driving moment; M_r, resisting moment; M_W, resisting moment about floodwall footing due to weights, W, of floodwall and the soils directly above floodwall footing; M_u, resisting moment about floodwall footing due to F_u; M_p, resisting moment about floodwall footing due to F_p; M_a, driving moment about floodwall footing due to F_a.

Because phase 1 of soil stockpile No.1 (4-m high) were formed about 6 months before the formation of phase 2 (10-m high) behind buildings 6-7, the subgrade would have undergone

consolidation for 6 months under the weight of the 4-m high stockpile. Consequently, the strength of the subgrade would have been enhanced to some extent. The detailed estimation of soil strength increment due to the consolidation is presented the later section entitled "Evaluation of Preloading Effect on the Soft Subgrade by the 4-m High Stockpile and will be not repeated herein.

Floodwall to the north of Building 6

Fig. S12 presents the configuration of the 10-m high stockpile N0.1 behind building 6, which was about 10 m to the south of the floodwall. Because of its trapezoidal cross-section geometry along the transverse direction, phase 1 and phase 2 of stockpile No.1 were simplified as two equivalent uniformly distributed strip loads in analysis, i.e., q_1 for phase 1 and q_2 for phase 2. The soil stockpiles had a unit weight about 16.5 $\mathrm{kN/m^3}$ and thus $q_1 = 16.5\ \mathrm{kN/m^3} \times 2.88\ \mathrm{m} = 47.5\ \mathrm{kP}$ and $q_2 = 16.5\ \mathrm{kN/m^3} \times 4.87\ \mathrm{m} = 80.3\ \mathrm{kPa}$. According to equations (S22) and (S23), σ_a behind the floodwall and σ_p in front of the floodwall were estimated and their magnitudes are summarized in Tables S6 to S8; the magnitudes of lateral addition earth pressures due to phase 1 and phase 2 of stockpile No.1 ($\Delta\sigma_{h1}$ and $\Delta\sigma_{h2}$) were calculated by equation (S25) and were summarized in Tables S9 and S10. Fig. S13 plots the distributions of the calculated σ_p and water pressure u in front of the floodwall and σ_a and $\Delta\sigma_h$ behind the floodwall; Fig. S14 presents the mechanical model for calculation of FS_3 and FS_4.

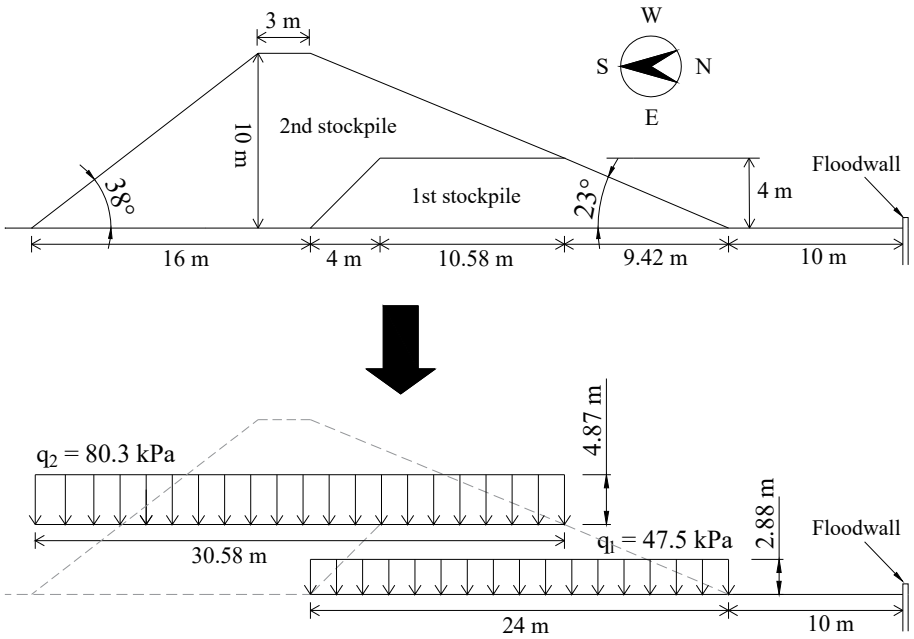

Fig. S12. Cross-section of stockpile No.1 behind building 6.

Table S6. The magnitudes of σ_p in front of the floodwall behind building 6.

Y (m)	γ (kN/m^3)	c_{cu} (kPa)	φ_{cu} (°)	K_p	σ_p (kPa)
0	15.8	8	14	1.64	20.48
2.5	15.8	8	14	1.64	85.19

Note: Y, depth below riverbed; γ, soil unit weight; c_{cu}, cohesion; φ_{cu}, friction angle.

Table S7. The magnitudes of σ_{a1} against floodwall behind building 6 without accounting for consolidation of the subsoil under the weight of the 4-m high stockpile.

Y (m)	γ (kN/m^3)	c_{cu} (kPa)	φ_{cu} (°)	K_a	σ_{a1} (kPa)
0	18.5	29	18.5	0.52	-41.75
0.5	18.5	29	18.5	0.52	-36.96
1	18.5	29	18.5	0.52	-27.37
2	17.9	18	12	0.55	0.78
3	17.9	18	12	0.55	12.52
4	15.8	8	14	0.61	35.94
5	15.8	8	14	0.61	45.58
6	15.8	8	14	0.61	55.22
7	15.8	8	14	0.61	64.87

Note: Y, depth below ground level.

Table S8. The magnitudes of σ_{a2} against floodwall behind building 6 accounting for consolidation of the subsoil for 6 months under the weight of the 4-m high stockpile.

Y (m)	γ (kN/m^3)	c* (kPa)	φ_{cu} (°)	K_a	σ_{a2} (kPa)
0	18.5	35.76	18.5	0.52	-51.49
0.5	18.5	35.76	18.5	0.52	-46.69
1	18.5	35.76	18.5	0.52	-37.11
2	17.9	24.76	22	0.55	-12.63
3	17.9	24.76	22	0.55	-4.49
4	15.8	14.76	14	0.61	25.37
5	15.8	14.76	14	0.61	35.02
6	15.8	14.76	14	0.61	44.66
7	15.8	14.76	14	0.61	54.31

Note: Y, depth below ground level; c*, soil cohesion considering the consolidation of the subsoils under the weight of the 4-m high stockpile for 6 months, refer to the section entitled "*Evaluation of Preloading Effect on the Soft Subgrade by the 4-m High Stockpile*" of this supplementary data.

Table S9. Magnitudes of $\Delta\sigma_{h1}$ against floodwall behind building 6 due to q_1.

Y (m)	x_i (m)	b + x_i (m)	q_1 (kPa)	β_1	β_2	$\Delta\sigma_{h1}$ (kPa)
0.5	10	34	47.5	1.56	1.52	1.07
1	10	34	47.5	1.54	1.47	2.12
2	10	34	47.5	1.51	1.37	4.12
3	10	34	47.5	1.48	1.28	5.92
4	10	34	47.5	1.45	1.19	7.44
5	10	34	47.5	1.42	1.11	8.68
6	8	32	47.5	1.39	0.93	11.45
7	8	32	47.5	1.36	0.85	11.95

Note: Y, depth below ground level.

Table S10. Magnitudes of $\Delta\sigma_{h2}$ against floodwall behind building 6 due to q_2.

Y (m)	x_i (m)	b + x_i (m)	q_2 (kPa)	β_1	β_2	$\Delta\sigma_{h2}$ (kPa)
0.5	19.42	50	80.3	1.56	1.55	0.79
1	19.42	50	80.3	1.55	1.52	1.58
2	19.42	50	80.3	1.53	1.47	3.14
3	19.42	50	80.3	1.51	1.42	4.65
4	19.42	50	80.3	1.49	1.37	6.09
5	19.42	50	80.3	1.47	1.32	7.43
6	17.42	48	80.3	1.45	1.24	9.89
7	17.42	48	80.3	1.43	1.19	11.10

Note: Y, depth below ground level.

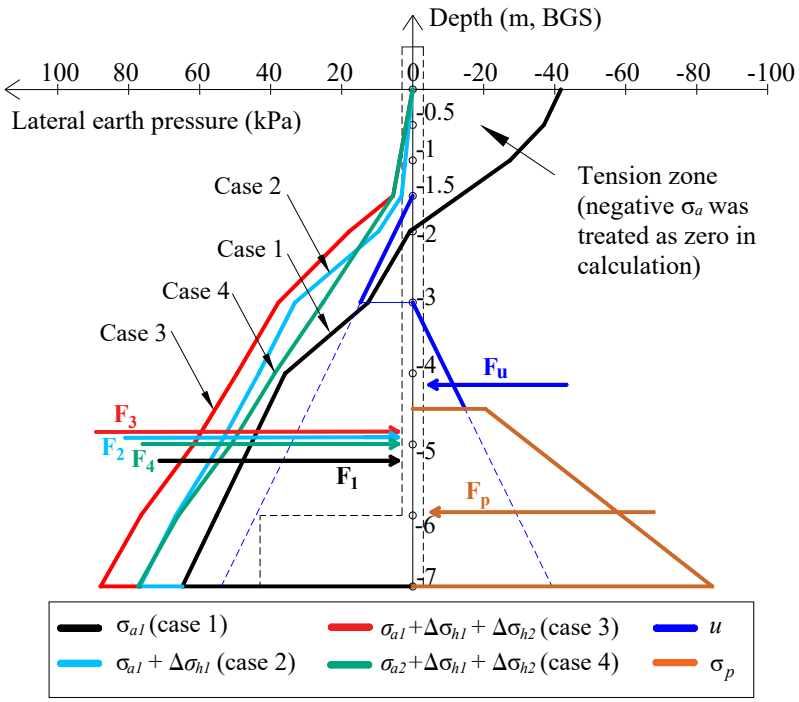

Fig. S13. Distribution of the calculated lateral earth pressures on the two sides of floodwall behind building 6 with respect to 4 different scenarios.

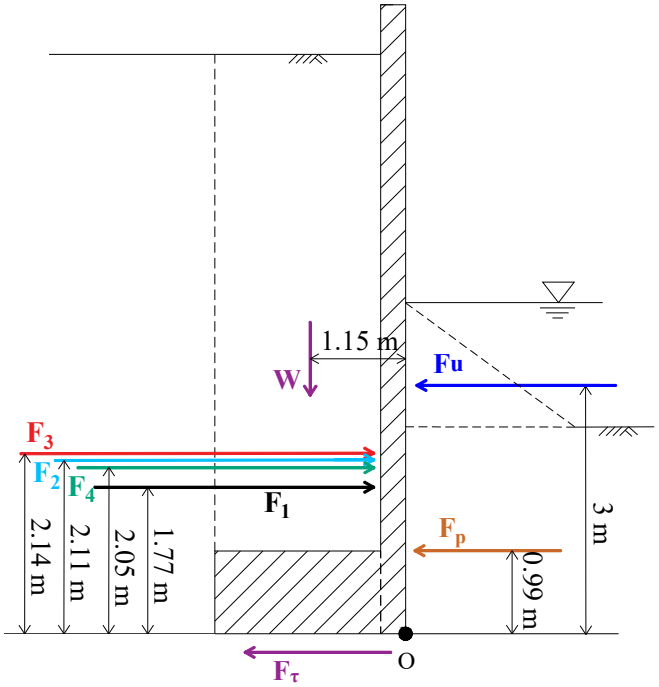

Fig. S14. Mechanical model for calculating FS_3 and FS_4 of floodwall behind building 6.

In Figs. S13 and S14, F_1 = thrust of lateral active earth pressure without stockpile nearby

(case 1); F_2 = thrust of lateral active earth pressure and additional lateral earth pressure caused by q_1 (case 2); F_3 = thrust of lateral active earth pressure and additional lateral earth pressure caused by (q_1+q_2) without accounting for consolidation of the subgrade under the weight of the 4-m high stockpile (case 3); F_4 = thrust of lateral active earth pressure and additional lateral earth pressure caused by (q_1+q_2) with accounting for consolidation of the subgrade for 6 months under weight of the 4-m high stockpile (case 4); F_u = thrust of water pressure above riverbed; F_p = thrust of lateral passive earth pressure below the riverbed. The calculated magnitudes of FS_3 and FS_4 with respect to cases 1-4 are summarized in Table S11.

Table S11. The estimated FS_3 and FS_4 for the floodwall behind building 6.

Scenarios	FS_3	FS_4
Case 1: Without stockpile behind floodwall	1.464	1.803
Case 2: After stockpiling the 4-m high soils (phase 1 of stockpile No.1) behind floodwall	1.045	1.084
Case 3: After stockpiling the 10-m high soils (phase 2 of stockpile No.1) behind floodwall (consolidation of the subsoils under the weight of the 4-m high stockpile for 6-months was not accounted for in analysis)	0.895	0.915
Case 4: After stockpiling the 10-m high soils (phase 2 of stockpile No.1) behind floodwall (consolidation of the subsoils under the weight of the 4-m high stockpile for 6-months was accounted for in analysis)	1.184	1.191

The calculations above indicated that if consolidation of the subgrade for 6 months under the weight of the 4-m high stockpile was not considered in the analyses (case 3), the floodwall behind building 6 would be subjected to both sliding and overturning failures . On the other hand, the calculated FS_3 and FS_4 were more than 1.0 (no sliding or overturning failure of

floodwall) when the preloading effect on subgrade were considered (case 4). The fact that the floodwall behind building 6 remained intact proved that the consolidation of the subgrade was a contributing factor to the stability of the floodwall

Floodwall to the North of Building 7

Fig. S15 presents the configuration of the stockpile No.1 behind building 7, which was about 10 m to the south of the floodwall. Because of its trapezoidal geometry along the transverse direction, phase 1 and phase 2 of stockpile No.1 were simplified as two equivalent uniformly distributed strip loads in the analysis, i.e., q_1 for phase 1 and q_2 for phase 2. The soil stockpile had a unit weight about 16.5 $\mathrm{kN/m^3}$ and thus $q_1 = 16.5\ \mathrm{kN/m^3} \times 2.88\ \mathrm{m} = 47.5\ \mathrm{kP}$ and $q_2 = 16.5\ \mathrm{kN/m^3} \times 5.29\ \mathrm{m} = 87.3\ \mathrm{kP}$. Using equations (S22) and (S23), σ_a behind the floodwall and σ_p in front of the floodwall can be estimated and their magnitudes along height are summarized in Tables S12 to S14; the magnitudes of lateral addition earth pressures due to phase 1 and phase 2 of the stockpile ($\Delta\sigma_{h1}$ and $\Delta\sigma_{h2}$) were calculated by equation (S25) and were summarized in Tables S15 and S16. Fig. S16 plots the distributions of the calculated σ_p and water pressure u in front of floodwall and σ_a and $\Delta\sigma_h$ behind floodwall; Fig. S17 presents the mechanical models for calculation of FS_3 and FS_4.

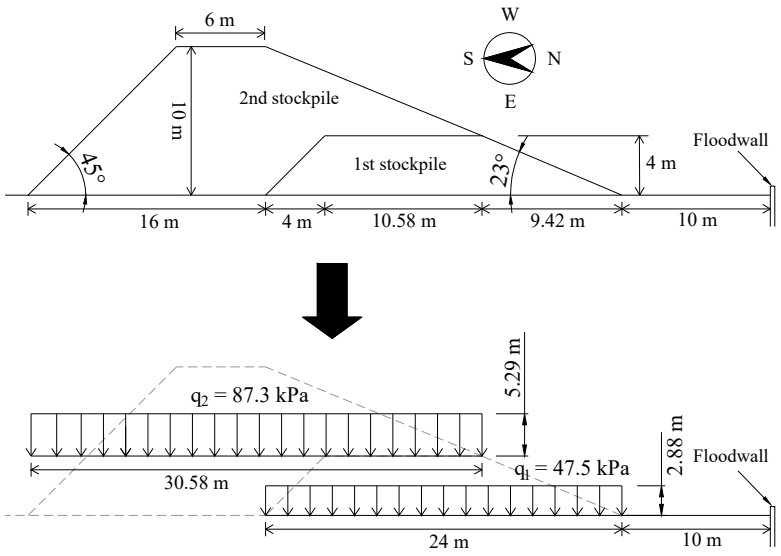

Fig. S15. Cross-section of stockpile No.1 behind building 7.

Table S12. The magnitudes of σ_p in front of the floodwall behind building 7.

Y (m)	γ (kN/m^3)	c_{cu}(kPa)	φ_{cu} (°)	K_p	σ_p (kPa)
0	15.6	8	14	1.64	20.48
2.5	15.6	8	14	1.64	84.37

Note: Y, depth below riverbed; γ, soil unit weight; c_{cu}, cohesion; φ_{cu}, friction angle.

Table S13. The magnitudes of σ_{a1} against floodwall behind building 7 without accounting for consolidation of the subsoil under weight of phase 1 of stockpile No.1.

Y (m)	γ (kN/m^3)	c_{cu} (kPa)	φ_{cu} (°)	K_a	σ_{a1} (kPa)
0	18.5	29	18.5	0.52	-41.75
0.5	18.5	29	18.5	0.52	-36.96
1	18.5	29	18.5	0.52	-27.37
2	19.7	14.5	22	0.55	-8.09
3	19.7	14.5	22	0.55	0.87
4	15.6	8	14	0.61	38.01
5	15.6	8	14	0.61	47.53
6	15.6	8	14	0.61	57.06
7	15.6	8	14	0.61	66.58

Note: Y, depth below ground level.

Table S14. The magnitudes of σ_{a2} against floodwall behind building 7 accounting for consolidation of the subsoil under weight of phase 1 of stockpile No.1.

Y (m)	γ (kN/m^3)	c* (kPa)	φ_{cu} (°)	K_a	σ_{a2} (kPa)
0	18.5	35.76	18.5	0.52	-51.49
0.5	18.5	35.76	18.5	0.52	-46.69
1	18.5	35.76	18.5	0.52	-37.11
2	19.7	28.76	22	0.55	-17.21
3	19.7	28.76	22	0.55	-8.25
4	15.6	14.76	14	0.61	27.45
5	15.6	14.76	14	0.61	36.97
6	15.6	14.76	14	0.61	46.49
7	15.6	14.76	14	0.61	56.01

Note: Y, depth below ground level; c*, soil cohesion considering the consolidation of the subsoils under the weight of the 4-m high stockpile for 6 months, refer to the later section entitled "*Evaluation of Preloading Effect on the Soft Subgrade by the 4-m High Stockpile*" of this supplementary data.

Table S15. Magnitudes of $\Delta\sigma_{h1}$ against floodwall behind building 7 caused by q_1.

Y (m)	x_i (m)	b + x_i (m)	q_1 (kPa)	β_1	β_2	$\Delta\sigma_{h1}$ (kPa)
0.5	10	34	47.5	1.56	1.52	1.07
1	10	34	47.5	1.54	1.47	2.12
2	10	34	47.5	1.51	1.37	4.12
3	10	34	47.5	1.48	1.28	5.92
4	10	34	47.5	1.45	1.19	7.44
5	10	34	47.5	1.42	1.11	8.68
6	8	32	47.5	1.39	0.93	11.45
7	8	32	47.5	1.36	0.85	11.95

Note: Y, depth below ground level.

Table S16. Magnitudes of $\Delta\sigma_{h2}$ against floodwall behind building 7 caused by q_2.

Y (m)	x_i (m)	b + x_i (m)	q_2 (kPa)	β_1	β_2	$\Delta\sigma_{h2}$ (kPa)
0.5	19.42	50	87.3	1.56	1.55	0.87
1	19.42	50	87.3	1.55	1.52	1.75
2	19.42	50	87.3	1.53	1.47	3.46
3	19.42	50	87.3	1.51	1.42	5.12
4	19.42	50	87.3	1.49	1.37	6.71
5	19.42	50	87.3	1.47	1.32	8.19
6	17.42	48	87.3	1.45	1.24	10.90
7	17.42	48	87.3	1.43	1.19	12.24

Note: Y, depth below ground level.

In Figs. S16 and S17, F_1 = thrust of lateral active earth pressure without stockpile nearby (case 1); F_2 = thrust of lateral active earth pressure and additional lateral earth pressure caused by q_1 (case 2); F_3 = thrust of lateral active earth pressure and additional lateral earth pressure caused by (q_1+q_2) without accounting for consolidation of the subgrade under the weight of 4-m high stockpile (case 3); F_4 = thrust of lateral active earth pressure and additional lateral earth pressure caused by (q_1+q_2) with accounting for consolidation of the subgrade under the weight of the 4-m high stockpile (case 4); F_u = thrust of water pressure; F_p = thrust of lateral passive earth pressure. The calculated magnitudes of FS_3 and FS_4 with respect to four different scenarios are summarized in Table S17.

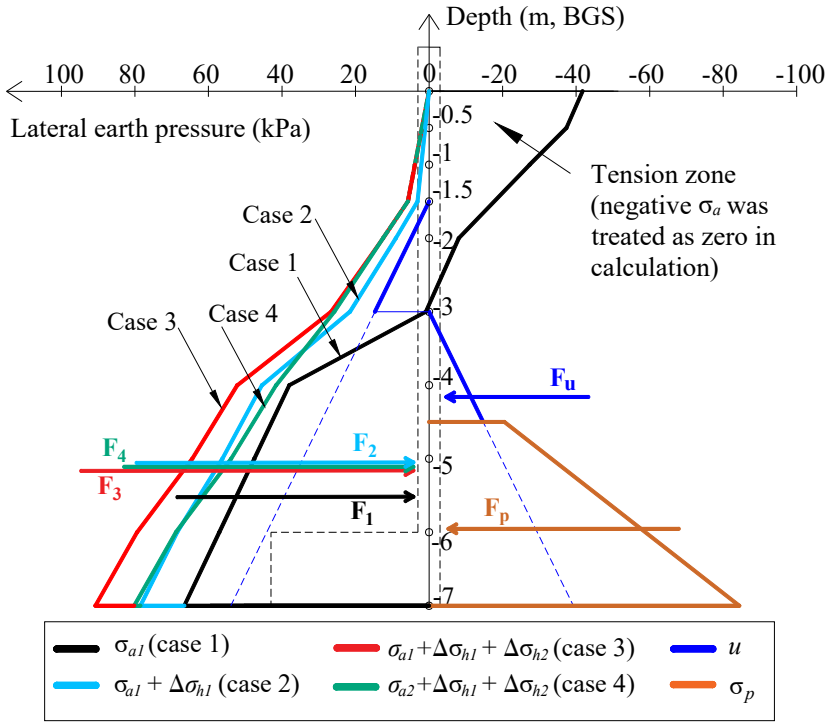

Fig. S16. Distribution of the calculated lateral earth pressures on the two sides of floodwall behind building 7 with respect to 4 different scenarios.

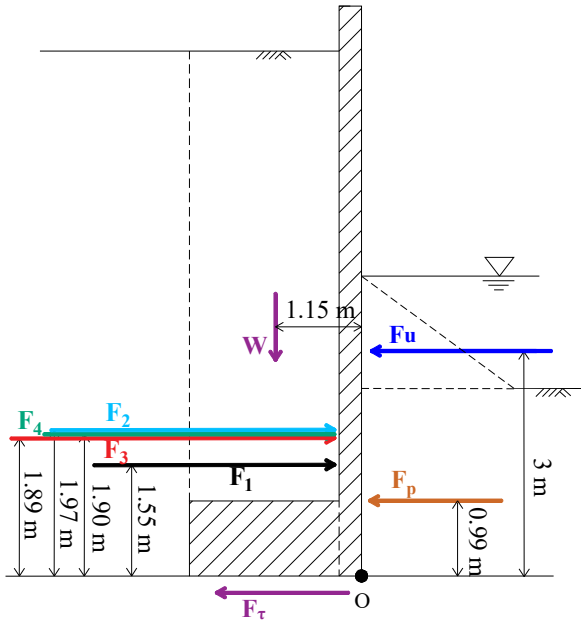

Fig. S17. Mechanical model for calculating FS_3 and FS_4 of floodwall behind building 7.

Table S17. The estimated FS_3 and FS_4 for the floodwall behind building 7.

Scenarios	FS_3	FS_4
Case 1: Without stockpile behind floodwall	1.505	2.165
Case 2: After stockpiling the 4-m high soils (phase 1 of stockpile No.1) behind floodwall	1.067	1.211
Case 3: After stockpiling the 10-m high soils (phase 2 of stockpile No.1) behind floodwall (consolidation of the subgrade under the weight of the 4-m high stockpile for 6-months was not accounted for in the analysis)	0.897	1.061
Case 4: After stockpiling the 10-m high soils (phase 2 of stockpile No.1) behind floodwall (consolidation of the subgrade under the weight of the 4-m high stockpile for 6-months was accounted for in the analysis)	1.121	1.229

If consolidation of the subgrade for 6 months under the weight of the 4-m high stockpile was not considered in analyses (case 3), sliding failure of the floodwall behind building 7 would be given by the calculations. This was contrary to the fact. However, if the preloading effect from the 4-m high stockpile on the subgrade were considered (case 4), both the calculated FS_3 and FS_4 were above 1.0 (neither sliding nor overturning failure would occur

for the floodwall), which was in agreement with the fact.

Floodwall to the North of Buildings 10-11

Fig. S18 presents the configuration of the 6-m high stockpile (stockpile No.2) behind buildings 10-11, which was about 6 m to the south of the floodwall. Because of its trapezoidal cross section geometry along the transverse direction, the stockpile was simplified as an equivalent uniformly distributed strip load, q, in analysis. The soil stockpile had a unit weight about 16.5 $\mathrm{kN/m^3}$ and thus $q = 16.5\ \mathrm{kN/m^3} \times 4.5\ \mathrm{m} = 74.25\ \mathrm{kP}$. According to equations (S22) and (S23), σ_a behind the floodwall and σ_p in front of the floodwall can be estimated and their magnitudes are summarized in Tables S18 to S19; the magnitudes of $\Delta\sigma_h$ due to the stockpile was calculated by equation (S25) and were summarized in Table S20. Fig. S19 plots the distributions of the calculated σ_p and water pressure u in front of floodwall and σ_a and $\Delta\sigma_h$ behind floodwall; Fig. S20 presents the mechanical models for calculation of FS_3 and FS_4.

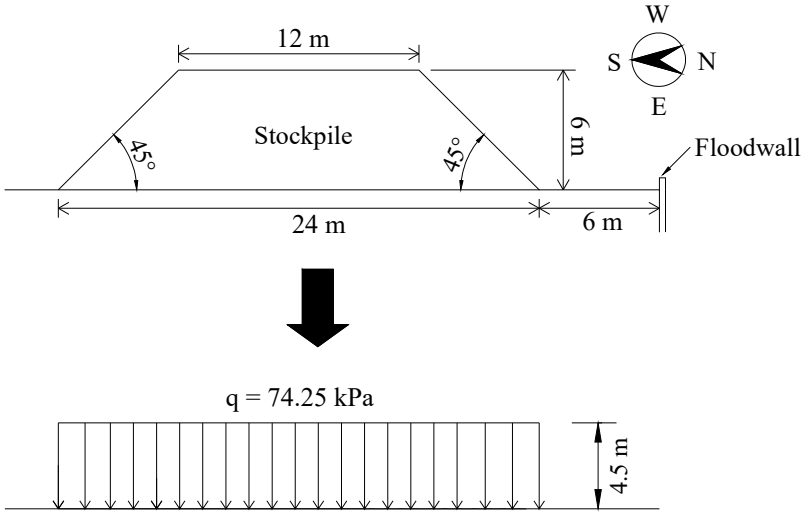

Fig. S18. Cross-section of stockpile No. 2 buildings 10 and 11.

Table S18. The magnitudes of σ_p in front of the floodwall behind buildings 10 and 11.

Y (m)	γ (kN/m^3)	c_{cu}(kPa)	φ_{cu} (°)	K_p	σ_p (kPa)
0	17.5	8	12	1.64	19.76
2.5	17.5	8	12	1.64	86.48

Note: Y, depth below riverbed; γ, soil unit weight; c_{cu}, cohesion; φ_{cu}, friction angle.

Table S19. The magnitudes of σ_a against floodwall behind buildings 10 and 11.

Y (m)	γ (kN/m^3)	c_{cu} (kPa)	φ_{cu} (°)	K_a	σ_a (kPa)
0	18.5	29	18.5	0.52	-41.75
0.5	18.5	29	18.5	0.52	-36.96
1	18.5	29	18.5	0.52	-27.37
2	17.9	14.5	17	0.55	3.54
3	17.9	14.5	17	0.55	13.34
4	17.5	8	12	0.61	40.19
5	17.5	8	12	0.61	51.67
6	17.5	8	12	0.61	63.14
7	17.5	8	12	0.61	74.62

Note: Y, depth below ground level.

Table S20. Magnitudes of $\Delta\sigma_h$ against floodwall behind buildings 10 and 11 caused by q.

Y (m)	x_i (m)	b + x_i	q (kPa)	β_1	β_2	$\Delta\sigma_h$ (kPa)
0.5	6	30	74.25	1.55	1.49	3.13
1	6	30	74.25	1.54	1.41	6.16
2	6	30	74.25	1.50	1.25	11.55
3	6	30	74.25	1.47	1.11	15.72
4	6	30	74.25	1.44	0.98	18.58
5	6	30	74.25	1.41	0.88	20.31
6	4	28	74.25	1.36	0.59	24.30
7	4	28	74.25	1.33	0.52	23.69

Note: Y, depth below ground level.

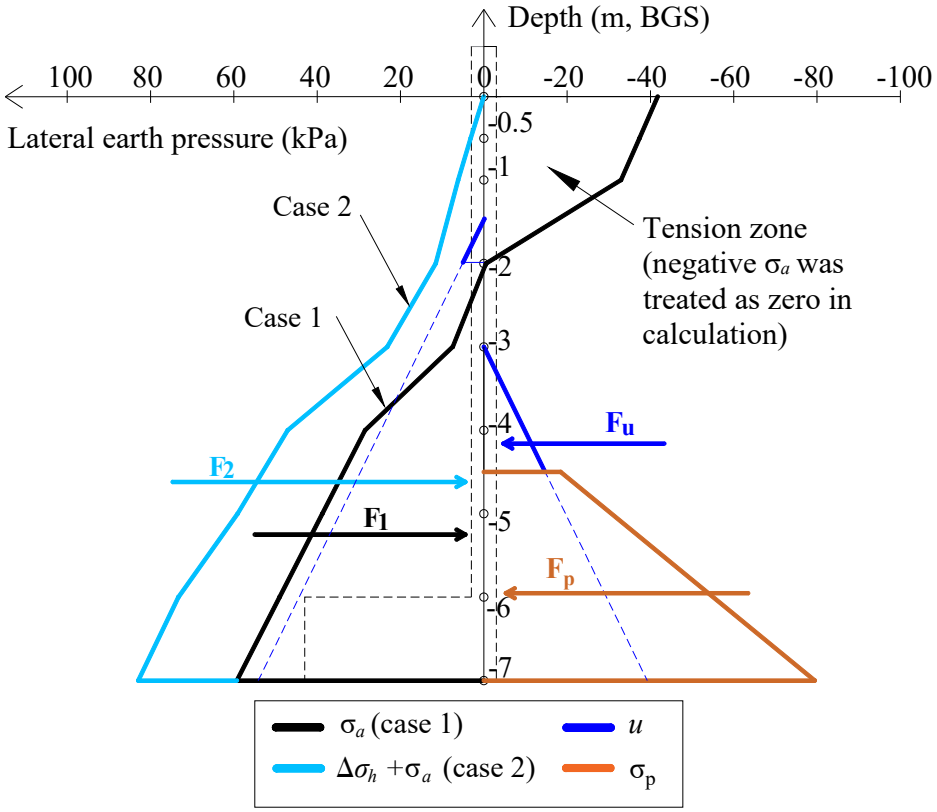

Fig. S19. Distribution of the calculated lateral earth pressures on the two sides of floodwall behind buildings 10 and 11 with respect to 2 different scenarios.

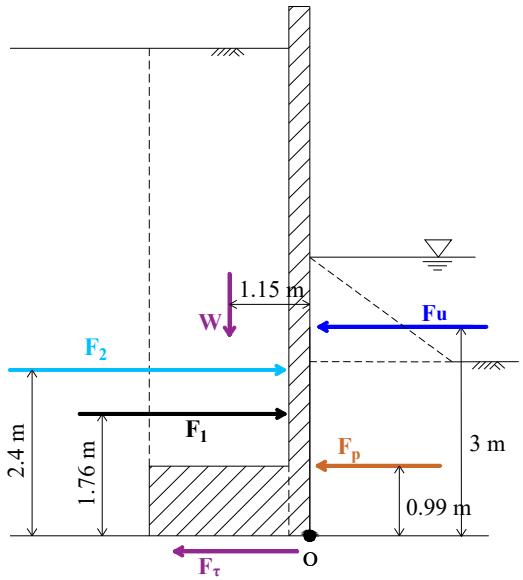

Fig. S20. Mechanical model for calculating FS_3 and FS_4 of floodwall behind buildings 10-11.

In Figs. S19 and S20, F_1 = thrust of lateral active earth pressure without stockpile nearby (case 1); F_2 = thrust of lateral active earth pressure and additional lateral earth pressure caused by q (case 2); F_u = thrust of water pressure above the riverbed; F_p = thrust of lateral passive earth pressure below the riverbed. The calculated magnitudes of FS_3 and FS_4 with respect to two different scenarios are summarized in Table S21.

Table S21. The estimated FS_3 and FS_4 for the floodwall behind buildings 10 and 11.

Scenarios	FS_3	FS_4
Case 1: Without stockpile behind floodwall	1.226	1.628
Case 2: After stockpiling the 6-m high soils behind floodwall	0.796	0.935

The calculation results indicated that with the presence of a 6-m high stockpile (stockpile No.2) nearby, the floodwall behind buildings 10-11 would undergo both sliding and overturning failures, which was consistent with the fact.

Evaluation of Preloading Effect on the Soft Subgrade by the 4-m High Stockpile

Consolidation Degree

As introduced in the manuscript, the excavated soils from the basement of building 11 were dumped on the landscaping area between buildings 5-7 and the Dingpu River to form a 3-4 m high stockpile about six months before the overturning failure of building 7. Under the weight of the stockpile (surcharge), consolidation of the underlying soft subgrade would take place and then the soil strength would be enhanced. Based on this consideration, consolidation degree of the subgrade (compressible sublayers 1-4), U_t, under the stockpile weight was estimated using the one-dimensional consolidation theory of Terzaghi (1943). Because of its trapezoidal geometry along the transverse direction, the 4-m high stockpile (phase 1 of stockpile No.1) was simplified as an equivalent load (2.88-m high rectangular stockpile) for analysis, see Fig. S21.

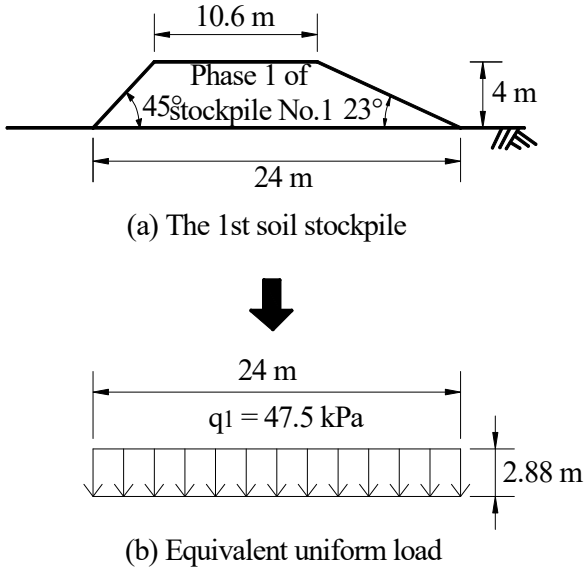

Fig. S21. Simplified model for calculation of equivalent load of the first 4-m high stockpile.

Since the stockpile had a unit weight, γ, of 16.5 kPa/m^3, the estimated equivalent load, q_1, was about 47.5 kPa. As recorded by the construction logs, the stockpiling was completed within 6 days and thus it was reasonably assumed that the underlying soft subgrade was in the undrained state during stockpiling and additional vertical earth pressure, $\Delta\sigma_v$, in the subgrade generated by stockpiling was fully carried by pore water first and then gradually carried by soil skeleton with dissipation of excess pore water pressure (consolidation), i.e.,

$$\Delta u_o = \Delta\sigma_v \tag{S29}$$

$$\Delta\sigma_{vi} = U_t \times \Delta u_o \tag{S30}$$

where, Δu_o, initial excess pore pressure generated by stockpiling; $\Delta\sigma_{vi}$, additional effective vertical earth pressure at time, *t*. $\Delta\sigma_v$ was estimated by Boussinesq solution for strip loading (Fig. S22) as below:

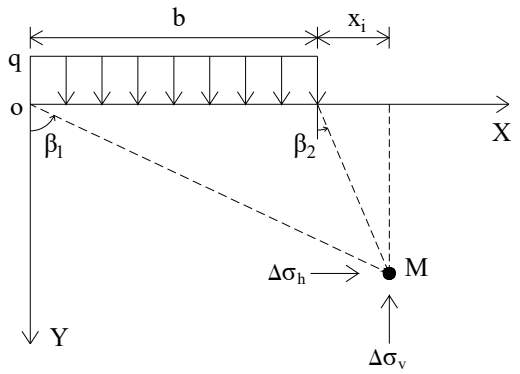

Fig. S22. Schematic illustration of calculation of $\Delta\sigma_v$ by Boussinesq solution for strip loading.

$$\Delta\sigma_v = \frac{q}{\pi}\left[\beta_1 + \frac{1}{2}\sin 2\beta_1 - \beta_2 - \frac{1}{2}\sin 2\beta_2\right] \tag{S31}$$

where, $q = q_1 = 47.5$ kPa. Therefore, the calculated $\Delta\sigma_v$ magnitudes at different depths, Y, along the vertical center line of the stockpile (x = b/2 = 12 m) are summarized in Table S22.

Table S22. $\Delta\sigma_v$ due to the 4-m high stockpile.

Y (m)	x_i (m)	b (m)	q (kPa)	β1	β2	$\Delta\sigma_v$ (kPa)
0	12	24	47.5	/	/	47.5
1	12	24	47.5	1.49	-1.49	47.5
2	12	24	47.5	1.41	-1.41	47.4
3	12	24	47.5	1.33	-1.33	47.2
4	12	24	47.5	1.25	-1.25	46.9
5	12	24	47.5	1.18	-1.18	46.3
6	12	24	47.5	1.11	-1.11	45.6
7	12	24	47.5	1.04	-1.04	44.7
8	12	24	47.5	0.98	-0.98	43.7
9	12	24	47.5	0.93	-0.93	42.6
10	12	24	47.5	0.88	-0.88	41.4
11	12	24	47.5	0.83	-0.83	40.1
12	12	24	47.5	0.79	-0.79	38.9
13	12	24	47.5	0.75	-0.75	37.6
13.8	12	24	47.5	0.72	-0.72	36.6

Since layer 5_1 (firm to stiff clay) directly below the upper compressible strata (layers 1-4) featured extremely lower vertical permeability ($k_v = 1 \times 10^{-9}$ m/s), the upper soft subgrade was only subjected to top (single) drainage instead of both top and bottom (double) drainage. By assuming a linear distribution of Δu_o along Y in the upper compressible strata, consolidation degree, U_t, of the upper subgrade can be estimated with the one-dimensional consolidation theory of Terzaghi (1943) as below:

$$U_t = 1 - \frac{(0.5 \cdot \pi \cdot \alpha - \alpha + 1)}{1+\alpha} \cdot \frac{32}{\pi^3} e^{-\frac{\pi^2}{4} T_v} \quad \text{(S32)}$$

$$\alpha = p_1/p_2 \quad \text{(S33)}$$

$$T_v = \frac{c_v \cdot t}{H^2} \quad \text{(S34)}$$

$$c_v = \frac{k_v \cdot E_s}{\gamma_w} \quad \text{(S35)}$$

where, p_1 and p_2 are the $\Delta\sigma_v$ magnitudes corresponding to Y = 0 and Y = 13.8 m in Table S22, respectively (p_1 = 47.5 kPa; p_2 = 36.6 kPa); T_v, time factor; c_v, coefficient of

consolidation; *H*, drainage length, equal to the height of the upper compressible subgrade; *t*, consolidation time; k_v, hydraulic conductivity in the vertical direction; E_s, constrained modulus of the upper subgrade; γ_w, unit water weight, equal to 9.8 $\mathrm{kN/m^3}$. For simplification, the weighted average k_v and E_s of layers 1-4 were adopted in calculation ($k_v = 3.29 \times 10^{-9}$ m/s; $E_s = 3.34$ MPa) and the estimated U_t = 0.38. This number matched well with that of one surcharge project near this site in Shanghai (Yang 2010), of which the measured U_t was 0.42 under a surcharge load of 60 kPa for 6 months.

Strength Increment due to Consolidation

Following consolidation (dissipation of excess pore water pressure over time), the compressible subgrade directly below the stockpile (surcharge) would gain strength increment over time. In this study, the strength increment, $\Delta\tau_f$, in soil shear strength was estimated by the method specified in Chinese Technical Code for Ground Treatment of Buildings, JGJ79-2002 (2002):

$$\Delta_{\tau_f} = \Delta\sigma_v \cdot U_t \cdot \tan\varphi \tag{S36}$$

φ, effective friction angle measured by consolidated undrained triaxial tests. In this study, φ was the weighted averaged magnitude of layers 1-4, equal to 20.63°. According to equation (S36), the calculated $\Delta_{\tau_f} = 6.76$ kPa.

Comprehensive Evaluations on Pile Capacities

All the 11 buildings at the investigated site were founded on lightly reinforced prestressed high-strength concrete (PHC) pipe piles (33-m in length, 400 mm in diameter and 80 mm in wall thickness). Fig. S23 schematically illustrated the cross section of the PHC piles in plane. All the piles were toed in the competent dense to very dense silty sand, i.e., end-bearing piles. According to the design logs, each pile had an allowable axial compression capacity of 1300 kN with a safety factor of 2.0, i.e., an ultimate axial compression bearing capacity, Q_{uk}, of 2600 kN (Netease 2009; Wang et al. 2017).

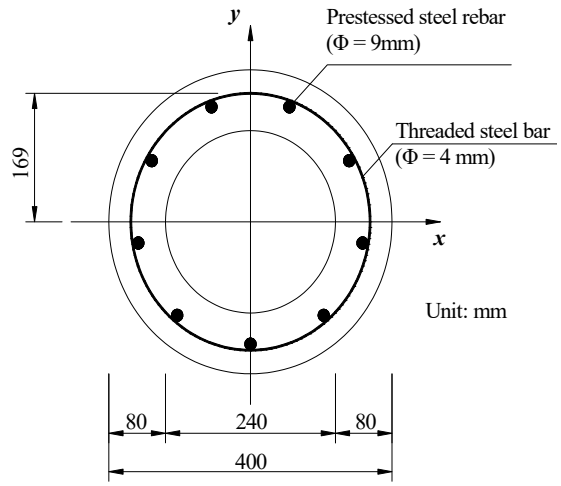

Fig. S23. Cross section of the PHC pipe piles adopted for the buildings at the site.

To verify the designed pile capacities, extensive calculations were conducted in the following paragraphs to evaluate pile cracking moment, M_r, ultimate bending moment, M_u, ultimate shear resistance, Q, ultimate compression (R_p) and tension (T_Q) strengths, and ultimate axial compression (Q_{uk}) and tension (T_{uk}) bearing capacities, according to Chinese Technical Code for Prestressed Concrete Pipe Piles, DGJ32/TJ109-2010 (2010).

Cracking Moment, M_r

The moment at which the PHC piles began to crack, M_r, was estimated by the method specified in DGJ32/TJ109-2010 (2010), i.e.,

$$M_r = \frac{I_p}{r_0}(\sigma_{pc} + \sigma_{cbt}) \tag{S37}$$

$$L_e = \frac{\pi}{4}(r_0^4 - r_i^4) + \frac{m}{2}A_p r_p^2 \tag{S38}$$

$$\sigma_{pc} = 0.6 n_s A_a \cdot F_{ptk}/A_j \tag{S39}$$

where, I_p, inertia moment of pile cross section; r_0, outer radius of pile, equal to 200 mm; σ_{pc}, effective prestress of pile; σ_{cbt}, concrete tension strength of pile subjected to bending, equal to 7.35 $\mathrm{N/mm^2}$; r_i, inner radius of pile, equal to 120 mm; m, ratio of steel elastic modulus to concrete elastic modulus, equal to 5.0; A_p, rebar area on pile cross section, equal to $A_p = 9A_a = 9 * \frac{\pi 9^2}{4} = 572.58\ \mathrm{mm^2}$; r_p, distance from pile center to steel rebar, equal to 169 mm; n_s, number of rebar in pile, equal to 9; A_a, cross-section area of one rebar, $A_a = \frac{\pi 9^4}{4} = 63.6\ \mathrm{mm^2}$; $A_j = \pi \times (r_o^2 - r_1^2) = 80424.77\ \mathrm{mm^2}$, area of pile rim; F_{ptk}, tensile strength of rebar, equal to 1420 MPa. According to equation (S37), the estimated M_r for the PHC piles of this site was about 76.1 kN · m.

Ultimate Bending Moment, M_u

The ultimate bending moment, M_u, of pile was calculated in accordance with equation (S40):

$$M_u = \alpha \cdot M_r \tag{S40}$$

where, α, ultimate coefficient proposed for PHC pile, equal to 1.65. The estimated $M_u = 1.65 \times 76.1 = 125.57$ kN · m.

Ultimate Shear Resistance, Q

The ultimate capacity of the PHC piles against shearing failure, Q, was estimated by equation (S41):

$$Q = \frac{2t \cdot I_p}{S_0} \cdot \frac{1}{2}\sqrt{(\sigma_{pc} + 2 \cdot \emptyset \cdot \sigma_t)^2 - \sigma_{pc}^2} \quad \text{(S41)}$$

where, t, pile wall thickness, equal to 80 mm; S_0, statical moment of pile cross section, $S_0 = \frac{2}{3} \times (r_0^3 - r_i^3) = 4.18 \times 10^6$ mm^3; r_o, outer radius of pipe pile, equal to 200 mm; r_i, inner radius of pipe pile, equal to 120 mm; $\emptyset$, dimensionless coefficient equal to d_o; d_o, outer diameter of pipe pile in meter; σ_t, tensile strength of prestressed concrete, equal to 5.39 N/mm^2. Therefore, the estimated $Q = 182.85$ kN.

Ultimate Compression Strength, R_p

The ultimate capability of the adopted PHC pipe piles against structural compression failure, R_p, was estimated by equation (S42):

$$R_p = 0.3(f_{ce} - \sigma_{pc})A_j \quad \text{(S42)}$$

where, f_{ce}, compression strength of concrete, equal to 80 MPa. The calculated $R_p =$ 1783.74 kN.

Ultimate Tensile Strength, T_Q

The ultimate capacity of the adopted PHC pipe piles against structural tension failure, T_Q, was estimated by equation (S43):

$$T_Q = \sigma_{pc} \cdot A_c = \sigma_{pc} \cdot （A_j - A_p） \quad \text{(S43)}$$

where, A_c, concrete area on pile cross section, $A_c = A_j - A_p$. The estimated $T_Q =$ 484.7 kN.

Ultimate Axial Compression Bearing Capacity

The ultimate axial compression bearing capacity of the adopted PHC pipe pile, Q_{uk}, was estimated by equation (S44):

$$Q_{uk} = Q_{sk} + Q_{pk} = u\sum q_{sik}\, l_i + q_{pk}(A_j + \lambda_p A_{p1}) \quad \text{(S44)}$$

where, Q_{sk}, side resistance; Q_{pk}, toe resistance; u, pile perimeter, $u = \pi d_0$; l_i, depth interval for each soil layer; q_{sik}, unit exterior side friction measured by CPT; q_{pk}, unit base resistance measured by CPT at the elevation of pile toe at 35 m BGS; $A_{p1} = \pi r_1^2$, open area of pile cross section; λ_p, empirical coefficient accounting for soil-plugging effect of open-ended pipe pile. λ_p was calculated by equations (S45) and (S46) as below:

$$\lambda_p = 0.16 h_b/d_0 \text{ when } h_b/d_0 < 5 \quad \text{(S45)}$$

$$\lambda_p = 0.8 \text{ when } h_b/d_0 \geq 5 \quad \text{(S46)}$$

where, h_b = pile embedment length in the bearing stratum - layer 7_{1-2}, equal to 2.2 m. $\frac{h_b}{d_0} = \frac{2.2}{0.4} = 5.5 > 5$; thus $\lambda_p = 0.8$ was adopted in calculation. According to equation (S44), the calculated $Q_{uk} = 2056.57$ kPa. Detailed calculation results are listed in Table S23.

Table S23. Calculation Table for Q_{uk}.

Soil Layer No. (Elevation, m)	l_i (m)	q_{sik} (kPa)	$uq_{sik}l_i$ （kN）	q_{pk} (kPa)
2 (2-3.5 m BGS)	1.50	15	28.28	
3 (5-6.0 m BGS)	2.50	15	47.14	
3 (6-7.5 m BGS)	1.50	18	33.94	
4 (7.5-13.5 m BGS)	6.00	20	150.84	
5_1 (13.5-19.2 m BGS)	5.70	35	250.77	

5_2 (19.2-21.5 m BGS)	2.30	45	130.10	
5_3 (21.5-28 m BGS)	6.50	40	326.82	
6 (28-29.7 m BGS)	1.70	60	128.21	
$7_{1\text{-}1}$ (29.7-32.8 m BGS)	3.10	70	272.77	
$7_{1\text{-}2}$ (32.8-35 m BGS)	2.20	80	221.23	4000
Pile length (m)	33.00	Q_{sk} (kN)	1590.11	
		Q_{pk} (kN)	466.46	
		Q_{uk} (kN)	2056.57	

Note: Pile head was located at 2 m below ground surface (BGS).

Ultimate Axial Tension Bearing Capacity

According to DGJ32/TJ109-2010 (2010), the ultimate axial tension bearing capacities of piles, T_{uk}, were calculated with respect to two cases, i.e., local and general tensile failures of pile group. For case 1 - local tensile failure of pile group,

$$T_{uk} = \frac{1}{n} u_l \sum \lambda_i q_{sik} l_i \quad \text{(S47)}$$

where, u_l, exterior perimeter of pile group, approximately $u_l = 2 \times (45 + 12) = 114$ m; n, number of piles, equal to 118.

For case 2 - general tensile failure of pile group,

$$T_{uk} = \sum \lambda_i \, q_{sik} u l_i \quad \text{(S48)}$$

where, λ_i, empirical pull-out coefficient proposed in DGJ32/TJ109-2010 (2010). The calculated T_{uk} was about 1068.83 kN for case 1 and 821.39 kN for case 2. Detailed calculations refer to Table S24 below.

Table S24. Calculation Table for T_{uk}.

Soil Layer No. (Elevation, m)	l_i (m)	q_{sik} (kPa)	λ_i	Case 1 (Local tensile failure) （kN）	Case 2 General tensile failure) （kN）
2 (2-3.5 m BGS)	1.50	15	0.70	19.80	15.21
3 (5-6.0 m BGS)	2.50	15	0.70	33.00	25.36
3 (6-7.5 m BGS)	1.50	18	0.70	23.76	18.26
4 (7.5-13.5 m BGS)	6.00	20	0.70	105.59	81.14
5_1 (13.5-19.2 m BGS)	5.70	35	0.70	175.54	134.90
5_2 (19.2-21.5 m BGS)	2.30	45	0.70	91.07	69.99
5_3 (21.5-28 m BGS)	6.50	40	0.70	228.77	175.81
6 (28-29.7 m BGS)	1.70	60	0.70	89.75	68.97
$7_{1\text{-}1}$ (29.7-32.8 m BGS)	3.10	70	0.70	190.94	146.74
$7_{1\text{-}2}$ (32.8-35 m BGS)	2.20	80	0.50	110.62	85.01
Pile length (m)	33.00	T_{uk}（kN）		1068.83	821.39

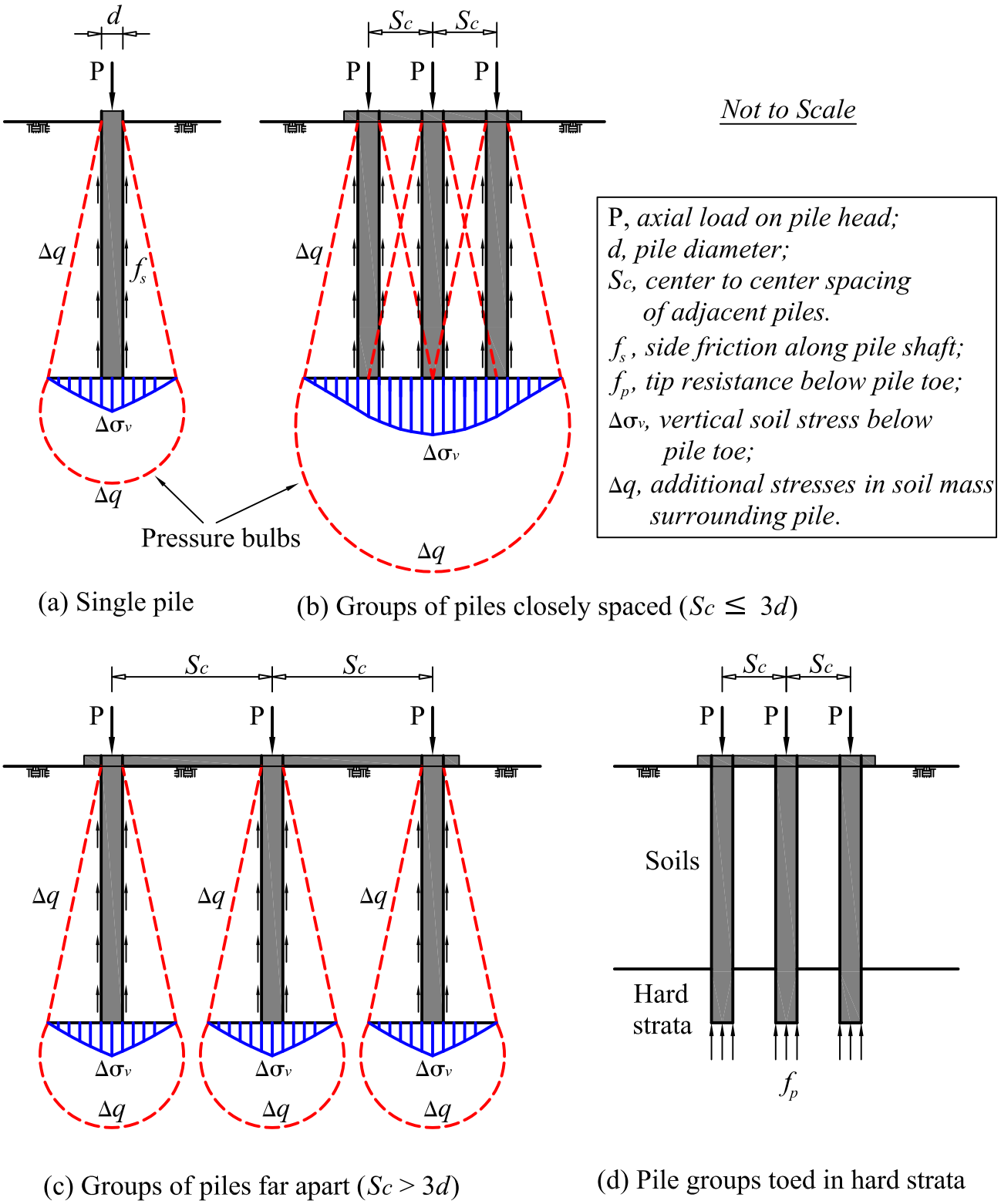

Fig. S24. Schematic illustration of pile-group effects on axial loading capacities of piles.

Evaluation of Overturning Moment Leading to Southward Rotational Failure of Building 7

During the abrupt toppling-failure of Building 7, the overturning moment, M_d, mainly arose from the general failure of the subgrade below the 10-m high stockpile about 1 m to the north of building 7 (ground heave below building basement and sliding failure of the stockpile directly behind); meanwhile, the weights of the building and the underlying piles, tensile force from the underlying piles, lateral passive earth pressures against the south side of the building basement and the southeast wind provided resisting moment, M_r, against southward tilting of building 7, see Fig. S25. Because building 7 fell to the ground, $M_d > M_r$. M_r can be estimated by equation (S49):

$$M_r = G\frac{w}{2} + \sum(T_Q + G_p)x + \sum f_w y + \sum \sigma_p y \qquad \text{(S49)}$$

where, G, buoyant weight of building; G_p, buoyant pile weight; T_Q, ultimate pile tensile strength; f_w, southeast wind load; σ_p, lateral passive earth pressure against south side of building basement; w, building width; x, lever arms of T_Q and G_p; y, lever arm f_{w} and σ_p around O. It should be pointed out that because the piles underwent tensile failure near pile head rather than the entire piles were pulled out (see Fig. 4 of the article), T_Q (ultimate pile tension strength) instead of T_{uk} (ultimate axial tension capacity) was adopted in equation (S49) for estimation of M_r.

Basic Information

Building 7 consisted of a 37.7-m high superstructure and 2-m deep basement and had a plan

dimension of 46.8 × 13.6 m. The building was founded on 118 PHC pipe piles (400 mm in diameter, 80 mm in wall thickness and 33 m in length); Fig. S26 presents the plane layout of the building foundation. At the time when rotational failure of building 7 occurred, there was southeast wind in-situ with a speed of about 9 m/s.

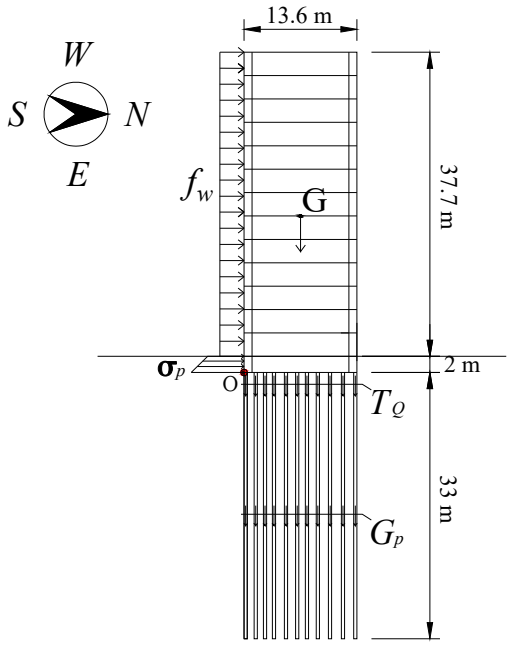

Fig. S25. Conceptual model for calculation of M_r.

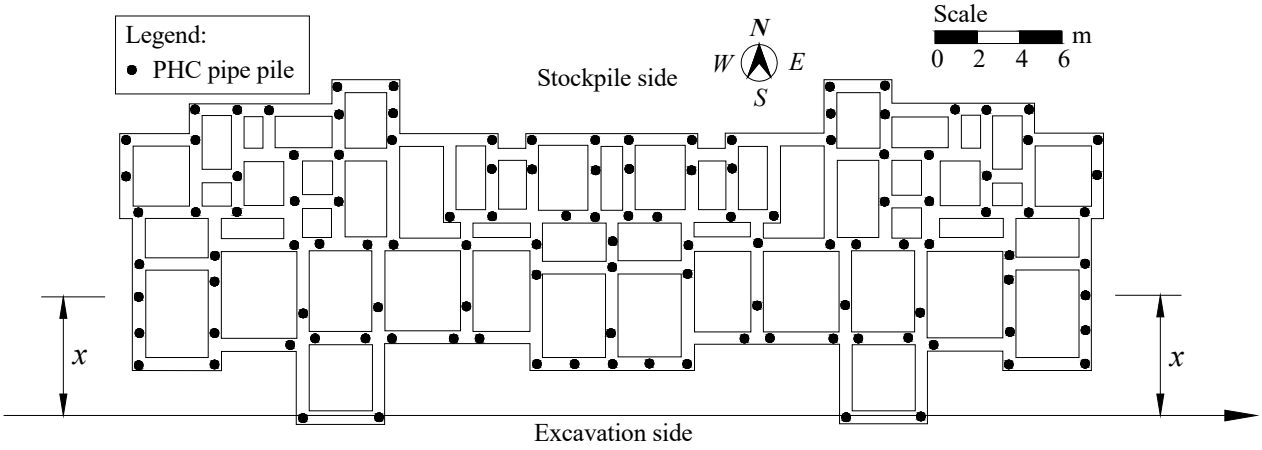

Fig. S26. Plane layout of the building footing.

Estimation on M_r

Resisting moment arising from pile tension

As aforementioned, because the piles underwent tensile failure near pile head rather than the entire piles were pulled out, T_Q instead of T_{uk} was adopted for estimation of the resisting moment. It has been estimated in Appendix V that the adopted PHC pipe piles had an ultimate tensile strength, T_Q, of 484.7 kN. The resisting moment of piles, M_{r1}, about the south edge of building 7, resulting from pile tension, can be calculated by:

$$M_{r1} = \sum n_i \times x \times T_Q \quad \text{(S50)}$$

where, n_i, number of piles at the same distance, x, normal to the south edge of building 7. The detailed calculation information and results are summarized in Table S25.

Table S25. Detailed calculation on M_{r1}.

i	x (m)	n_i	M_{r1} (kN·m)
1	0	4	0.00
2	2.13	9	9291.70
3	2.90	2	2811.26
4	3.14	10	15219.58
5	3.30	1	1599.51
6	3.38	4	6553.14
7	4.15	2	4023.01
8	4.43	4	8588.88
9	4.83	2	4682.20
10	5.39	2	5225.07
11	5.67	2	5496.50
12	5.92	1	2869.42
13	6.08	2	5893.95
14	6.44	2	6242.94
15	6.84	12	39784.18
16	6.96	1	3373.512
17	7.93	4	15374.68
18	7.97	4	15452.24
19	8.09	6	23527.34
20	8.53	4	16537.96
21	9.54	4	18496.15

22	9.78	2	9480.73
23	9.82	4	19039.02
24	10.38	4	20124.74
25	10.99	12	63922.24
26	11.99	4	23246.21
27	12.15	6	35334.63
28	13.08	4	25359.50
Total	/	118	407550.30

Resisting moment arising from pile weight

The long-term phreatic water level in Shanghai was around 1.50 m BGS and located at about 2.5-3.2 m BGS at this site. As marked in Fig. S25, the piles were located below 2 m. It The full lengths of the piles were almost buried below water level and hence would sustain upward buoyant force, F_w. Thus, the buoyant weight of each pile, G_p, can be calculated by:

$$G_p = G_{pile} - F_w \tag{S51}$$

where, G_{pile}, pile weight. G_{pile} was calculated by:

$$G_{pile} = \gamma_c \times V_{pile} \tag{S52}$$

$$V_{pile} = \frac{1}{4}\pi[d_0^2 - (d_0 - 2t)^2]L_{pile} \tag{S53}$$

in which, γ_c, unit weight of concrete, equal to 25 $\mathrm{kN/m^3}$; V_{pile}, concrete volume of PHC pipe pile; d_0, outer diameter of PHC pipe pile, equal to 400 mm; *t*, wall thickness of PHC pipe pile, equal to 80 mm; L_{pile}, pile length, equal to 33 m. According to equation (S52), the calculated $G_{pile} =$ 66.25 kN. Considering soil plugging of precast concrete pipe pile formed during its installation by driving, F_w for each PHC pipe pile can be calculated by:

$$F_w = \gamma_w \times \frac{1}{4}\pi d_0^2 L_{pile} = 41.47 \text{ kN} \tag{S54}$$

where, γ_w, unit weight of water, equal to 9.8 $\mathrm{kN/m^3}$. Then, the calculated $G_p = 66.25 - 41.47 = 24.78$ kN for each pile. Consequently, resisting moment, M_{r2}, arising from pile

weight can be calculated by:

$$M_{r2} = \sum n_i \times x \times F_w \quad \text{(S55)}$$

where, n_i, number of piles at the same distance, x, normal to the south edge of building 7. Detailed calculations of M_{r2} are summarized in Table S26.

Table S26. Detailed calculation on M_{r2}.

i	x (m)	n_i	M_{r2} (kN·m)
1	0	4	0.00
2	2.13	9	475.03
3	2.9	2	143.72
4	3.14	10	778.09
5	3.3	1	81.77
6	3.38	4	335.03
7	4.15	2	205.67
8	4.43	4	439.10
9	4.83	2	239.37
10	5.39	2	267.13
11	5.67	2	281.01
12	5.92	1	146.70
13	6.08	2	301.32
14	6.44	2	319.17
15	6.84	12	2033.94
16	6.96	1	172.47
17	7.93	4	786.02
18	7.97	4	789.99
19	8.09	6	1202.82
20	8.53	4	845.49
21	9.54	4	945.60
22	9.78	2	484.70
23	9.82	4	973.36
24	10.38	4	1028.87
25	10.99	12	3267.99
26	11.99	4	1188.45
27	12.15	6	1806.46
28	13.08	4	1296.49
Total	/	118	20835.77

Resisting moment arising from building weight

Building 7 was a 14-story structure, consisting of a 13-story superstructure and an underground basement (2 m high); each floor had an area of 430 m^2 with a unit load of 14 kN/m^2. Thereby, the total weight, G_b, of building 7 can be calculated by:

$$G_b = 430\ \mathrm{m}^2 \times 14\ \mathrm{kN/m}^2 \times 14 = 84280\ \mathrm{kN} \quad \text{(S56)}$$

As mentioned previously, the phreatic water level at this site was located at 2.5-3.2 m BGS. Thus, the building basement was above the phreatic water level and sustained buoyant force, $F_{wb} = 0.0$.

Then, the resisting moment by the building weight can be calculated by:

$$M_{r3} = G_b \times 0.5 w_b \quad \text{(S57)}$$

where, w_b, building width, equal to 13.6 m. The calculated $M_{r3} = 573164\ \mathrm{kN \cdot m}$.

Resisting moment arising from the southeast wind

According to the record of local weather station, there was a southeast wind with a maximum velocity of 9 m/s at the time of building failure, see Fig. 10 of the article. Because southeast wind was in the direction of southeast to northwest, the wind load on the south facade of building 7 would provide resisting moment, M_{r4}, against southward inclination of building 7. According to the relationship curve between wind velocity and wind load in Fig. S27 proposed by Chinese Technical Code for Highrise Concrete Superstructure - JGJ3-2010 (2010), a unit wind load, f_w, of 50 N/m^2 can be determined for this case. Then, M_{r4} can be calculated by equation (S58):

$$M_{r4} = \sum f_w y = f_w \times H \times L \times (0.5H + H_b) \quad \text{(S58)}$$

where, y, lever arm of wind load; H, height of superstructure, equal to 37.7 m; L, building length, equal to 46.8 m; H_b, height of building basement, equal to 2 m. The calculated $M_{r4} = 1839.35\ \text{kN} \cdot \text{m}$.

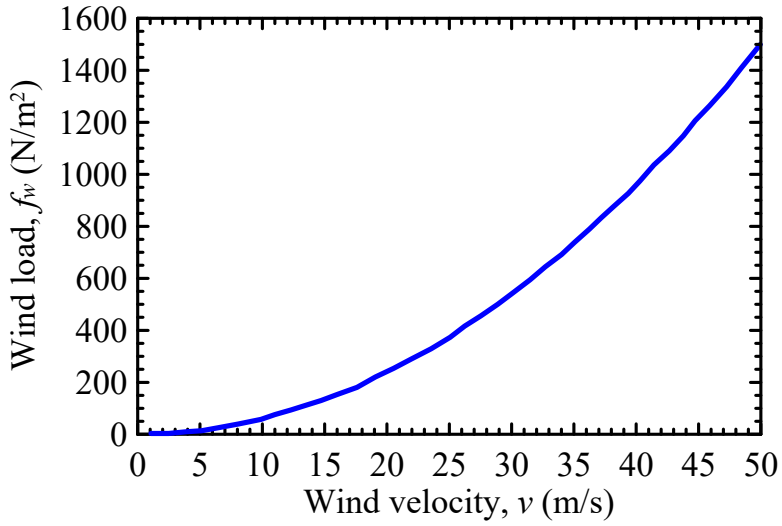

Fig. S27. Relationship between wind velocity and wind load.

Resisting moment arising from lateral earth pressure against south side of building basement

At the time point of building tilting, the soil mass on the south side of the building basement was in the passive state. Thereby, the lateral earth resistance against the south side of the building basement (2 m high) can be estimated by Rankine passive earth pressure theory, i.e.,

$$\sigma_p = \gamma z K_p + 2c_{cu}\sqrt{K_p} \tag{S59}$$

where, γ, soil unit weight; z, depth below ground surface; $K_p = tan^2(45° + \frac{\varphi_{cu}}{2})$; φ_{cu}, soil friction angle measured by consolidated undrained direct simple-shear test; c_{cu}, soil cohesion measured by consolidated undrained direct simple-shear test. The soil parameters used in calculation are listed in Table S27. Fig. S28 plots the distribution of the calculated σ_p against

the south side of the building basement.

Table S27. Soil parameters used in calculation of lateral earth pressure.

Soil layer	Stratum thickness (m)	γ (kN/m^3)	c_{cu} (kPa)	φ_{cu} (°)	K_p
1	1.3	18.5	29	18.5	1.93
2	0.7	19.7	22	22.0	2.20

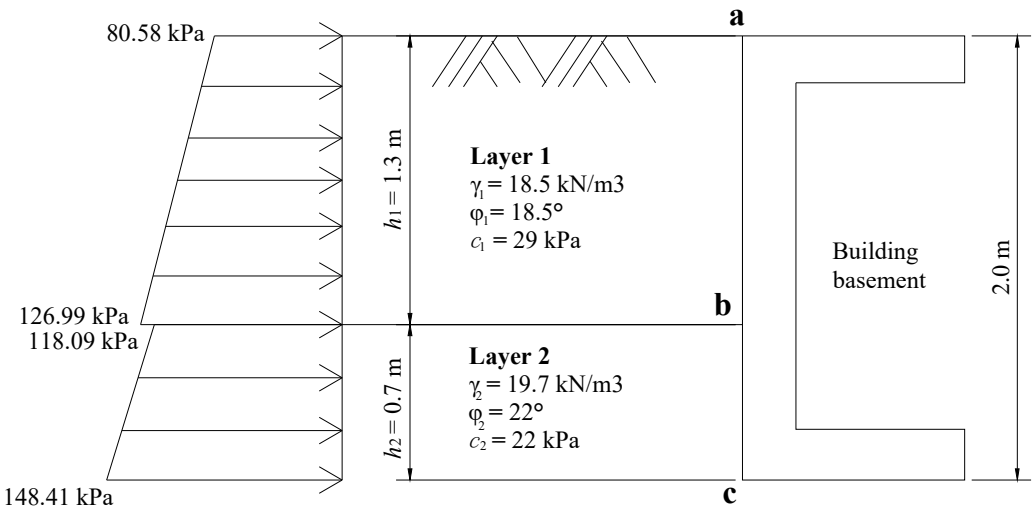

Fig. S28. Distribution of the calculated σ_p along depth.

At point **a** at ground level, $\sigma_p = 2c_1\sqrt{K_{p1}} = 80.58$ kPa;

At point **b** of layer 1 (1.3 m below ground level): $\sigma_{p1} = \gamma_1 h_1 K_{p1} + 2c_1\sqrt{K_{p1}} = 126.99$ kPa;

At point **b** of layer 2 (1.3 m below ground level): $\sigma_{p2} = \gamma_2 h_2 K_{p2} + 2c_2\sqrt{K_{p2}} = 118.09k$Pa;

At point **c** (2.0 m below ground level), $\sigma_p = (\gamma_1 h_1 + \gamma_2 h_2)K_{p2} + 2c_2\sqrt{K_{p2}} = 148.41k$Pa.

Based on the distribution of σ_p along depth, the resultant force, E_p, of σ_p against the south side of the building basement can be calculated as below:

$$E_p = \left(80.58 \times 1.3 + \frac{1}{2} \times (126.99 - 80.58) \times 1.3\right) + \left(118.09 \times 0.7 + \frac{1}{2} \times (148.41 - 118.09) \times 0.7\right) =$$
$$104.75 + 30.17 + 82.66 + 10.61 = 228.2 \text{ kN/m} \quad \text{(S60)}$$

The normal distance, y, between E_p and the toe of the building basement is equal to:

$$\text{y} = \frac{1}{228.2} \times (104.75 \times 1.35 + 30.17 \times 1.133 + 82.66 \times 0.35 + 10.61 \times 0.233) = 0.907 \text{ m} \quad \text{(S61)}$$

Therefore, the resisting moment, M_{r5}, of σ_p against southward overturning of building 7 can

be calculated by:

$$M_{r5} = L_b \times E_p \times y \quad \text{(S62)}$$

where, L_b, building length along longitudinal direction, equal to 46.8 m. The calculated $M_{r5} = 9686.54\ \text{kN} \cdot \text{m}$.

Total Resisting Moment against Southward Tilting of Building 7

Based on the calculation results above, the total resisting moment, M_r, against southward tilting of building 7, which derived from pile tension force, buoyant weights of the underlying piles and the building, the southeast wind and the lateral earth pressure against south side of the 2-m high building basement, can be obtained as below:

$$M_r = M_{r1} + M_{r2} + M_{r3} + M_{r4} + M_{r5} \quad \text{(S63)}$$

The relevant results are summarized in Table S28.

Table S28. Summary of the Calculated M_r against Southward Tilting of Building 7.

Resisting Moment	M_r (kN·m)
M_{r1}	407550
M_{r2}	20836
M_{r3}	573104
M_{r4}	1839
M_{r5}	9687
M_r	1013016

3D Numerical Simulations – Material Parameters and Typical Results

Undoubtedly, southward overturning failure of building 7 inherently correlated with the 10-m high soil stockpile about 1 m to its north. However, it was questionable that the abrupt southward falling over of building 7 arose from the unequal lateral earth pressures on the two sides of building 7. According to the pressure bulb theory (Lambe and Whitman 1969), those piles closer to the stockpile sustained much larger additional earth pressures from the stockpile than the piles distant away; moreover, the influence zone of the shallow excavation (4.6 m) 7 m distant from the building hardly reached the building, refer to Fig. 2 of the article. Thus, it can be deduced that the piles underneath the north building side would have deflected and settled much more than the piles underneath the south building side; consequently, the building would have tilted northwards to the stockpile rather than southwards to the excavation subjected to the additional earth pressures generated by the stockpile.

To verify this deduction, three-dimensional (3D) numerical simulation were conducted. The material parameters used in the FE simulations were presented below. Moreover, some typical FE simulation results were provided as supplementary data for reference.

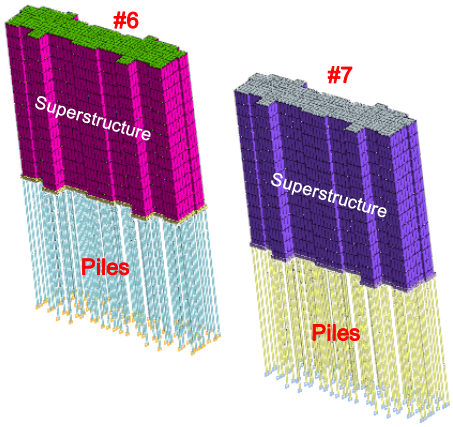

Fig. S29. 3D view of the building models adopted in numerical simulation.

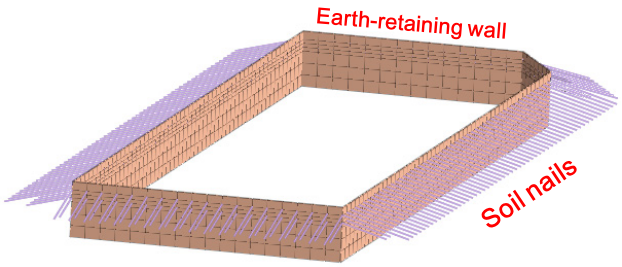

Fig. S30. 3D view of the earth-supporting systems for simulation of excavation.

Table S29. Soil parameters used in numerical simulation.

Stratum No.	h (m)	γ (kN/m^3)	v	K_o	E_{50}^{ref} (MPa)	E_{oed}^{ref} (MPa)	E_{ur}^{ref} (MPa)	R_f	c_{cu} (kPa)	φ_{cu} (°)	m
1	1.3	18.5	0.33	0.49	4.88	3.75	21.39	0.91	29.0	18.5	0.8
2	2.2	19.7	0.40	0.67	6.56	5.05	28.78	0.91	22.0	22.0	0.8
3	4.0	15.6	0.45	0.82	1.52	1.17	10.60	0.68	7.0	12.0	0.8
4	6.0	17.1	0.47	0.89	2.18	1.98	14.30	0.72	7.0	17.0	0.8
5_1	5.7	17.9	0.40	0.67	3.96	4.40	19.80	0.89	14.5	21.0	0.8
5_2	2.3	18.4	0.40	0.67	6.53	7.25	32.63	0.89	10.0	28.7	0.8
5_3	6.5	19.0	0.40	0.67	4.06	4.51	20.30	0.89	16.5	17.3	0.8
6	1.7	19.6	0.40	0.67	8.51	9.46	25.54	0.90	35.0	18.0	0.8
$7_{1\text{-}1}$	3.1	19.4	0.37	0.59	8.85	8.85	26.54	0.90	12.0	27.5	0.5
$7_{1\text{-}2}$	7.2	18.7	0.35	0.54	11.02	11.02	33.06	0.90	7.0	30.0	0.5
7_2	10.0	19.0	0.30	0.43	17.77	17.77	53.51	0.90	6.0	31.5	0.5

Note: h, stratum thickness; γ, soil unit weight; v, Poisson's ratio; K_o, lateral earth pressure coefficient at rest; E_{50}^{ref}, secant stiffness; E_{oed}^{ref}, tangent stiffness; E_{ur}^{ref}, unloading / reloading stiffness; R_f, strength reduction factor; c_{cu}, cohesion; φ_{cu}, friction angle; m, K_o related parameter.

Table S30. Material Parameters of Structural Elements Used in 3D Modeling.

Structural elements	Soil-mixing -wall	Soil nails	PHC pipe piles	Bottom plate	Laminate plate and exterior wall	Shear wall	Ground beam
Material	Soil cement	Q235 steel	C80 concrete	C40 concrete	C30 concrete	C30 concrete	C40 concrete
Unit type	2D shell	1D implantable truss	1D beam	2D shell	2D shell	2D shell	3D shell
Model type	Elastic	Elastic	Elastic	Elastic	Elastic	Elastic	Elastic
Elastic modulus (MPa)	120	2×10^5	3.8×10^4	3.25×10^4	3×10^4	3×10^4	3.25×10^4

Poisson ratio	0.2	0.3	0.2	0.2	0.2	0.2	0.23
γ (kN · m^{-3})	19	78	25	0	0	0	25
Section size	Thickness = 0.7 m	Outer diameter = 48 mm; Thickness = 3 mm	Outer diameter = 0.4 m; Thickness = 80 mm	Thickness = 0.35 m	Thickness = 0.2 m	Thickness = 0.3 m	Height = 0.7 m

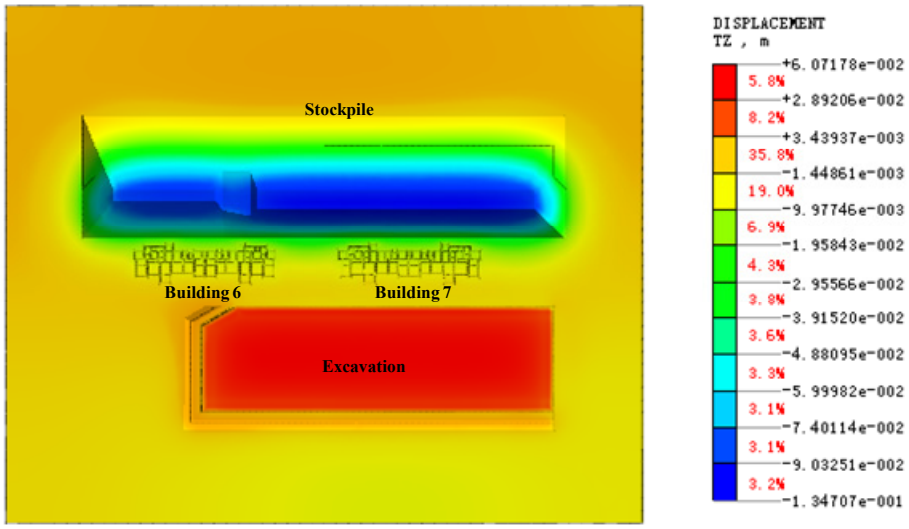

Fig. S31. Top-view of the simulated vertical displacement field at the site (*Note: negative magnitudes represent settlement; positive magnitudes represent heave*).

The simulated lateral and vertical building displacements at the completion of excavation and stockpiling indicated a northward instead of southward inclination of buildings 6-7. The simulated northward inclinations were about 0.091% for building 6 and 0.10% for building 7, both of which were much less than the specified 0.2% by Chinese Technical Code for Highrise Concrete Superstructure – JGJ3-2010 (2010). Moreover, both the simulated maximum bending moment ($M = 56.4\ \text{kN} \cdot \text{m}$) and shear force ($Q = 49.5\ \text{kN}$) at the completion of stockpiling were much smaller than their design magnitudes ($M_u = 125.57\ \text{kN} \cdot \text{m};\ Q = 182.85\ \text{kN}$), refer to Fig. S32. There did not exist a possibility of

shearing or bending failure of underlying piles resulting from southward lateral ground displacement underneath building 7, as claimed by the preceding investigations (Netease 2009; Yin and Xu 2009; Khudeira 2010; Wang et al. 2017).

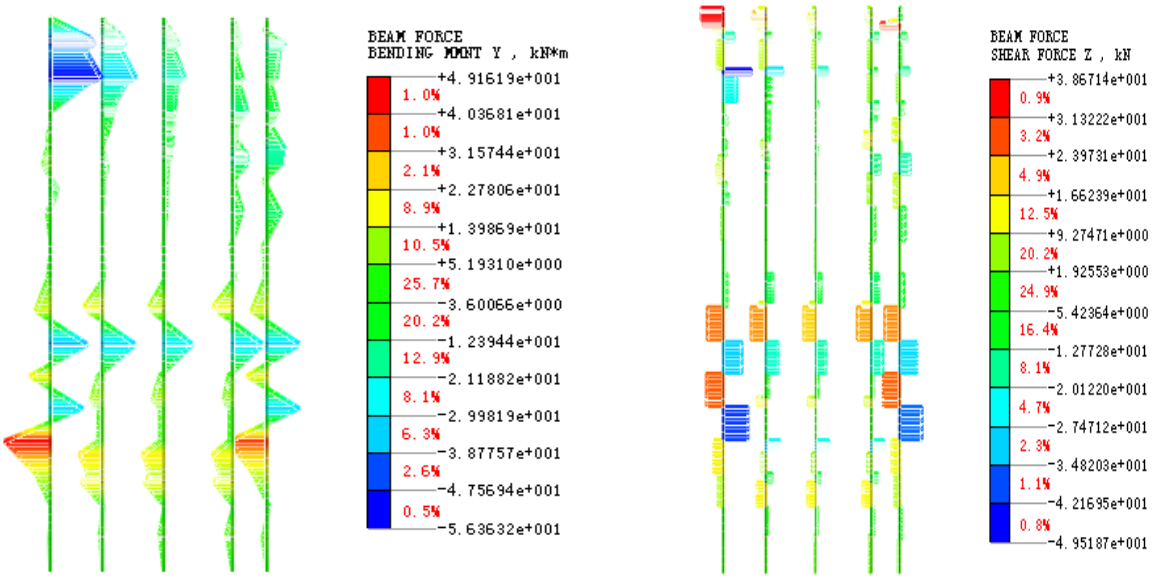

(a) Maximum bending moment of piles. (b) Maximum shear force of piles.

Fig. S32. Simulated maximum bending moment and shear force of the piles below building 7 along north-south direction.

Once again, the 3D numerical simulation results verify the deductions, i.e., before the abruptly falling over of building 7, both buildings 6 and 7 would have tilted slightly northwards rather than southwards at the completion of 4.6-m deep excavation and dumping of the 10-m high stockpile. Apparently, there was no possibility that the abrupt failure of building 7 was incurred by either the uneven earth pressure conditions beneath buildings 6-7 (Netease 2009; Yin and Xu 2009; Khudeira 2010) or greater settlement of the piles underneath the south building side than that of the piles below the north building side (Chai et al. 2014; Wang et al. 2017).

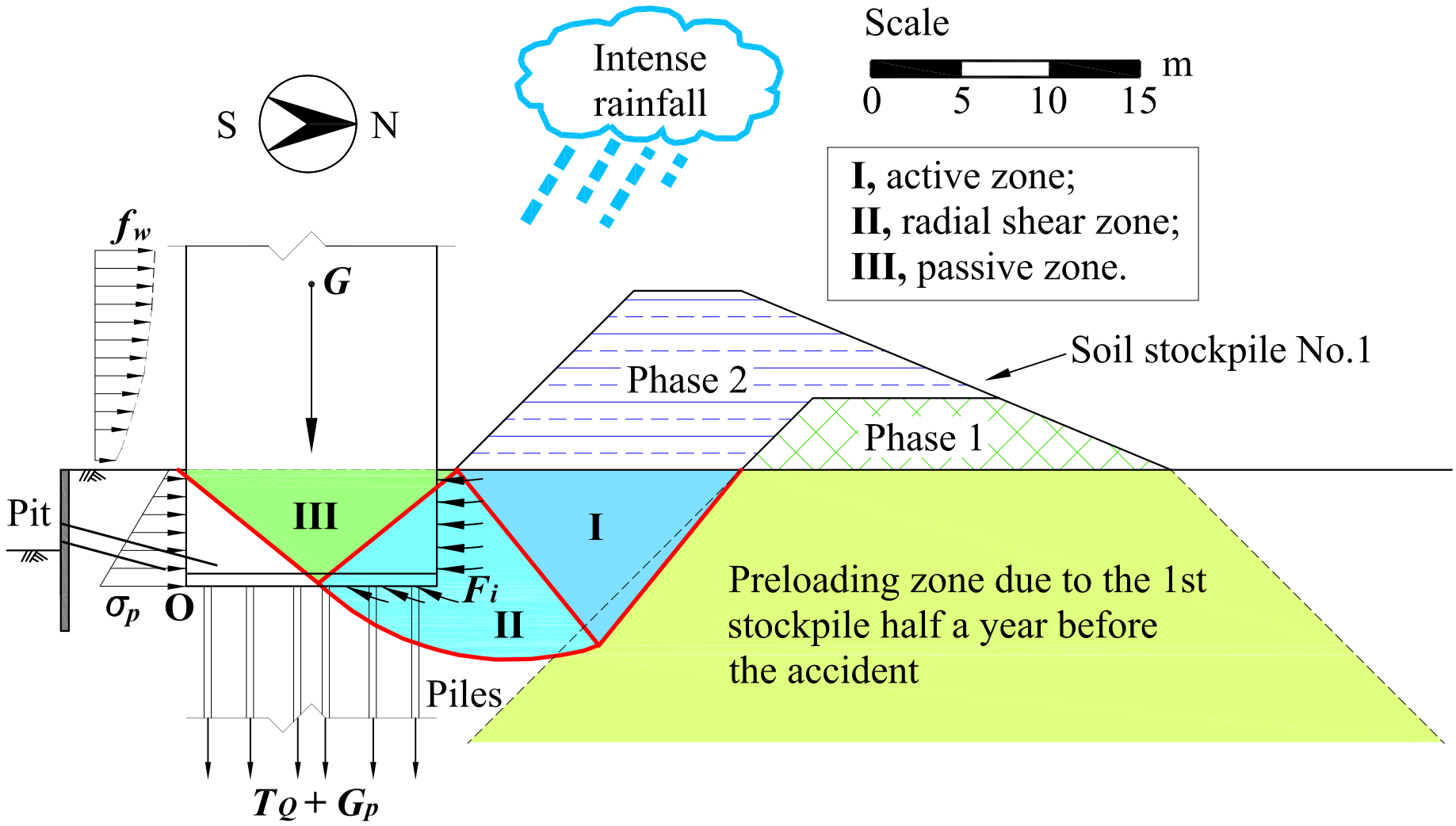

Fig. S33. Schematic illustration of bearing-capacity-failure scenario in case of an embedment depth of 6.6 m for the building footing.

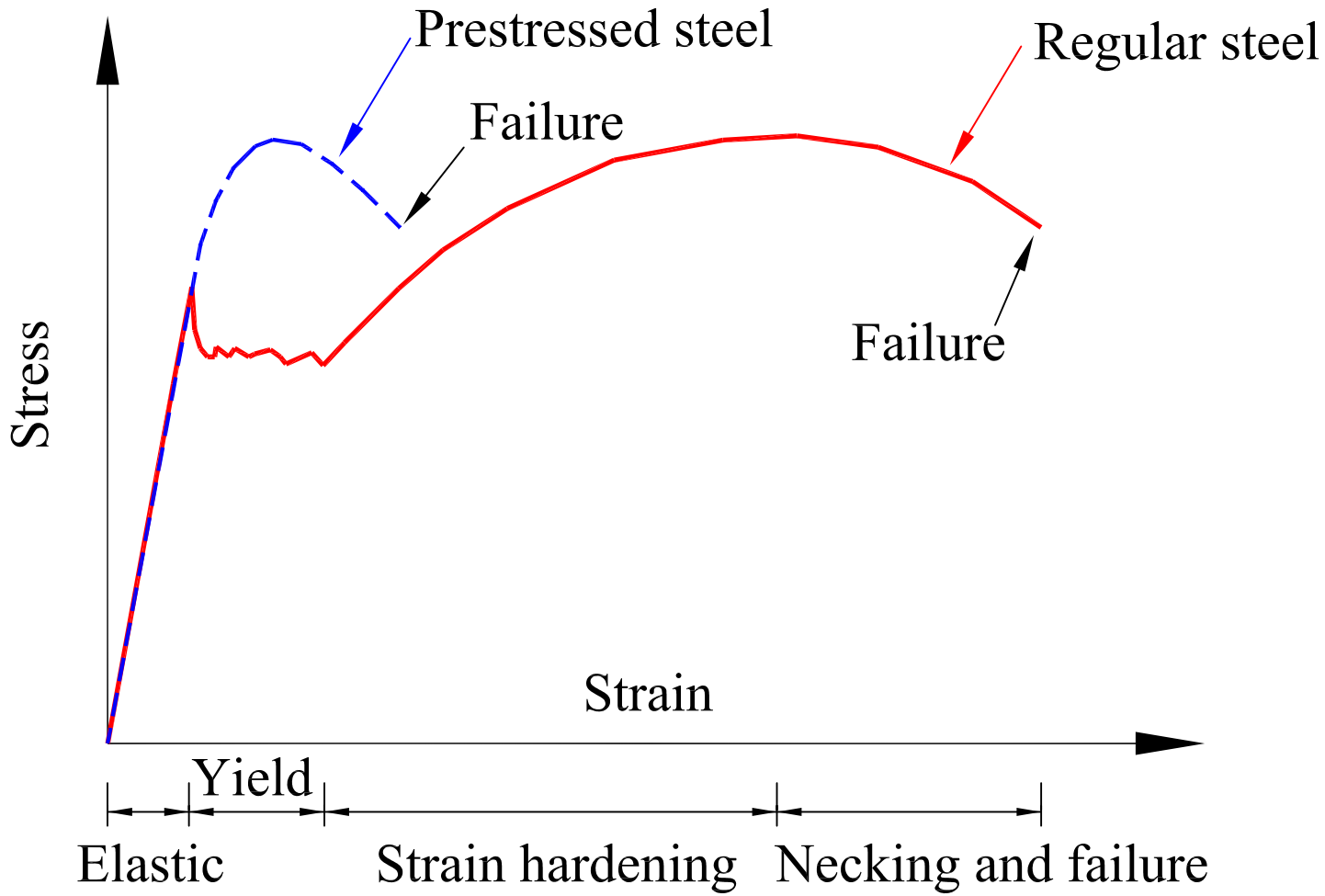

Fig. S34. Typical stress-strain curves of regular steel and prestressed steel.

References

Burd, H. J., and S. Frydman. 1997. “Bearing capacity of plane-strain footings on layered soils.” *Can. Geotech. J.* 34: 241-253.

Chai, J., S. Shen, W. Ding, H. Zhu, and J. Carter. 2014. “Numerical investigation of the failure of a building in Shanghai, China.” *Computers and Geotechnics* 55: 482-493.

Das, B. M., and K. Sobhan. 2017. Principals of Geotechnical Engineering (9th Edition), Cengage Learning, ISBN-13: 978-1305970953.

DGJ32/TJ109-2010. 2010. Technical Code for Prestressed Concrete Pipe Pile Foundation, Jiangsu Department of Housing and Rural Development, Nanjing, China (In Chinese).

Fellenius, B. H. 1984. “Negative skin friction and settlement of piles.” *Second International Seminar, Pile Foundations*, Nanyang Technological Institute, Singapore.

Fellenius, B. H. 1998. “Recent advances in the design of piles for axial loads, dragloads, downdrag, and settlement.” *Proceedings of ASCE and Port of NY and NJ Seminar*.

GB/T 50805-2012. 2012. Chinese Code for Design of Urban Flooding Control Project, Ministry of Water Resources of China, China Planning Press, Beijing (In Chinese).

GTS NX. 2014. *Midas GTS NX User Manual*, GTS NX, Republic of Korean.

JGJ3-2010. 2010. Technical Code for Highrise Concrete Superstructure, the Ministry of Construction of China, Beijing (In Chinese).

JGJ79-2002. 2002. Technical Code for Ground Treatment of Buildings, China Academy of Building Research, Beijing, China (In Chinese).

Khudeira, S. 2010. “Building collapse during construction.” *Pract. Period. Struct. Des. Constr.*, 15(2): 99-100.

Lambe, T. W., and R. V. Whitman. 1969. *Soil Mechanics*, New York, John Wiley & Sons, Inc.

Liu, Q. S., and J. Yu. 2017. "Calculation of ultimate bearing capacity of the man-made crust over dredged waste dump sites." *China Harbour Engineering* 37(9): 32-37 (In Chinese with English Abstract).

Michalowski, R. 1992. "Bearing capacity of nonhomogeneous cohesive soils under embankments." *J. Geotech. Engrg.* 118(7): 1098-1118.

Michalowski, R. L. 2004. "Limit loads on reinforced foundation soils." *J. Geotech. Geoenv. Engrg.* 130(4): 381-390.

Netease. 2009. Primary Factor Triggering Falling Over of the Building within Lotus Riverside Neighborhood: Lateral Ground Movement Arising from Unequal Lateral Earth Pressure Conditions, 163 News, July 4, 2009, Shanghai, China (In Chinese).

Prandtl, L. 1920. "Uber die Harte plastischer Korper". *Gotinger Nachrichten*, Math.-Phys., 74-85 (In German).

SXGEI. 2006. *Geotechnical Exploration Report for Lotus Riverside Resident Neighborhood (No. 2005-03-22)*, Shanghai Xie-Li Geotechnical Engineering Investigation Co., Ltd., Shanghai, China (In Chinese).

Terzaghi, K. 1943. Theoretical Soil Mechanics, New York, John Wiley & Sons, Inc.

Wang, W. D., Q. Li, Y. Hu, J. W. Shi, and C. W. W. Ng. 2017. "Field investigation of collapse of a 13-story high-rise residential building in Shanghai." *J. Perform. Constr. Facil.* 31(4): 04017012.

Wei, X., J. Zheng, and L. Wu. 2012. "Failure model of soft clay hard shell layer foundation." *Journal of Highway and Transportation Research and Development* 29(8): 31-37 (In

Chinese with English Abstract).

Yang, S. F. 2010. “Disciplines of foundation deformation under large area earth loading.” *Shanghai Geology* (1): 16-20 (In Chinese with English Abstract).

Yin, J., and F. Xu. 2009. “3D numerical analysis of the overturning of a residential under construction in Shanghai.” *Proceedings of annual meeting of geotechnical engineering in Shanghai*, 152-156 (In Chinese with English Abstract).